Molecular Pharmacology Fast Forward. Published on September 9, 2021 as DOI: 10.1124/molpharm.121.000290
This article has not been copyedited and formatted. The final version may differ from this version.

High-content single-cell FRET imaging of cultured striatal neurons reveals novel cross-talk in the regulation of nuclear signalling by PKA and ERK1/2

Jace Jones-Tabah[1], Ryan D. Martin[1], Jason C. Tanny[1], Paul B.S. Clarke[1]* and Terence E. Hébert[1]*

[1]Department of Pharmacology and Therapeutics, McGill University, Montréal, Québec, H3G 1Y6, Canada

Molecular Pharmacology Fast Forward. Published on September 9, 2021 as DOI: 10.1124/molpharm.121.000290
This article has not been copyedited and formatted. The final version may differ from this version.

Running title: High-content single-cell FRET imaging of striatal neurons

* Co-corresponding authors- address correspondence to:

Dr. Terence E. Hébert, PhD,

Department of Pharmacology and Therapeutics,

McGill University,

3655 Promenade Sir-William-Osler, Room 1303

Montréal, Québec, H3G 1Y6, Canada

Tel: (514) 398-1398

E-mail: terence.hebert@mcgill.ca

OR

Dr. Paul Clarke, PhD,

Department of Pharmacology and Therapeutics,

McGill University,

3655 Promenade Sir-William-Osler, Room 1325

Montréal, Québec, H3G 1Y6, Canada

Tel: (514) 398-3616 ext 1

E-mail: paul.clarke@mcgill.ca

Number of pages: 41

Number of figures: 9

Number of references: 48

Number of words, Abstract: 248

Number of words, Introduction: 690

Number of words, Discussion: 1498

Molecular Pharmacology Fast Forward. Published on September 9, 2021 as DOI: 10.1124/molpharm.121.000290
This article has not been copyedited and formatted. The final version may differ from this version.

Abbreviations:

AKAP: A-kinase anchoring protein
AKAR: A-kinase activity reporter (FRET biosensor)
AMPK: AMP-activated protein kinase
AAV: adeno-associated virus
cAMP: cyclic adenosine monophosphate
CFP: cyan fluorescent protein
DARPP-32: dopamine-and-cAMP regulated phosphoprotein of 32 kDa
D1R: dopamine receptor subtype D1
D2R: dopamine receptor subtype D2
EKAR: ERK kinase activity reporter (FRET biosensor)
ERK: extracellular signal regulated kinase
FRET: Förster resonance energy transfer
HBSS: Hanks balanced salt solution
L-DOPA: levodopa, l-3,4-dihydroxyphenylalanine
MEK: MAPK and ERK kinase
MSN: medium spiny GABAergic projection neuron
NES: nuclear export signal
NLS: nuclear localization signal
NMDA: *N*-Methyl-D-aspartic acid
PBS: phosphate-buffered saline
PDE: phosphodiesterase
PKA: protein kinase A
PMA: phorbol-12-myristate-13-acetate
YFP: yellow fluorescent protein

Molecular Pharmacology Fast Forward. Published on September 9, 2021 as DOI: 10.1124/molpharm.121.000290
This article has not been copyedited and formatted. The final version may differ from this version.

Abstract (250 word max)

Genetically-encoded biosensors can be used to track signaling events in living cells by measuring changes in fluorescence emitted by one or more fluorescent proteins. Here, we describe the use of genetically-encoded biosensors based on Förster resonance energy transfer (FRET) combined with high-content microscopy, to image dynamic signaling events simultaneously in thousands of neurons in response to drug treatments. We first applied this approach to examine intercellular variation in signaling responses among cultured striatal neurons stimulated with multiple drugs. Using high-content FRET imaging and immunofluorescence, we identified neuronal sub-populations with unique responses to pharmacological manipulation, and used nuclear morphology to identify medium spiny neurons within these heterogeneous striatal cultures. Focusing on PKA and ERK1/2 signaling in the cytoplasm and nucleus, we noted pronounced intercellular differences among putative medium spiny neurons, in both the magnitude and kinetics of signaling responses to drug application. Importantly, a conventional “bulk” analysis that pooled all cells in culture yielded a different rank order of drug potency than that revealed by single-cell analysis. Using a single-cell analytical approach, we dissected the relative contributions of PKA and ERK1/2 signalling in striatal neurons and unexpectedly identified a novel role for ERK1/2 in promoting nuclear activation of PKA in striatal neurons. This finding adds a new dimension of signalling crosstalk between PKA and ERK1/2 with relevance to dopamine D1 receptor signaling in striatal neurons. In conclusion, high-content single-cell imaging can complement and extend traditional population-level analyses and provides a novel vantage point from which to study cellular signaling.

Molecular Pharmacology Fast Forward. Published on September 9, 2021 as DOI: 10.1124/molpharm.121.000290
This article has not been copyedited and formatted. The final version may differ from this version.

Molecular Pharmacology Fast Forward. Published on September 9, 2021 as DOI: 10.1124/molpharm.121.000290
This article has not been copyedited and formatted. The final version may differ from this version.

Significance Statement: (1-2 sentences and 80-word maximum)

High-content imaging revealed substantial intercellular variation in the magnitude and pattern of intracellular signaling events driven by receptor stimulation. Since individual neurons within the same population can respond quite differently to a given agonist, interpreting measures of intracellular signaling derived from the averaged response of entire neuronal populations may not always reflect what happened at the single cell level. We used this approach to identify a new form of cross-talk between PKA and ERK1/2 signaling in the nucleus of striatal neurons.

Molecular Pharmacology Fast Forward. Published on September 9, 2021 as DOI: 10.1124/molpharm.121.000290
This article has not been copyedited and formatted. The final version may differ from this version.

Introduction

Neurons in the dorsal striatum regulate goal-directed locomotion, behavioural action selection, and specific forms of learning. Medium spiny GABAergic projection neurons (MSNs) account for 95% of the neurons found in the rodent striatum (Ivkovic and Ehrlich, 1999; Schambra et al., 1994). These neurons integrate dopaminergic and glutamatergic inputs to the striatum and send inhibitory projections to several downstream nuclei. Based on both anatomical and molecular features, MSNs are broadly divided into two subpopulations: "direct pathway" MSNs, which express the $G\alpha_{s/olf}$-coupled D1 dopamine receptor (D_1R), and "indirect pathway" MSNs, which express the $G\alpha_{i/o}$-coupled D2 receptor (D_2R) (Thibault et al., 2013; Gerfen et al., 1990). Recent studies using single-cell transcriptomics have demonstrated that even *within* these primary striatal subpopulations, variable expression of distinct molecular features can further define distinct sub-classes (Gokce et al., 2016; Märtin et al., 2019; Saunders et al., 2018; Stanley et al., 2020). However, the *functional* consequences of this transcriptional diversity remain unexplored. In the present study, we were interested in understanding diversity in signaling responses to drugs among neurons belonging to a single striatal population, i.e. MSNs. More specifically, we sought to answer two main questions: firstly, how much do individual MSNs differ in their signaling responses to pharmacological manipulation, and secondly, how does this variability inform our understanding of the way drugs act on these cells?

In addition to dopamine receptors, both of the predominant MSN subtypes also express NMDA-sensitive glutamate receptors (NMDARs) (Flores-Hernández et al., 2002; Mao et al.,

Molecular Pharmacology Fast Forward. Published on September 9, 2021 as DOI: 10.1124/molpharm.121.000290
This article has not been copyedited and formatted. The final version may differ from this version.

2004). In MSNs that form the direct pathway, the D_1R and NMDAR cooperatively regulate synaptic plasticity and gene expression through activation of PKA and ERK1/2 protein kinases (Paul et al., 2000; Saxena et al., 1999; Valjent et al., 2005). Activation of these intracellular signaling pathways by D_1R and NMDAR plays an important role, for example, in the effects of cocaine, which increases both dopamine and glutamate in the striatum (Fasano et al., 2009; Pascoli et al., 2011). However, little is known about intercellular heterogeneity in PKA or ERK1/2 responses. Interestingly, in a recent study using single cell transcriptomics, only a small proportion of molecularly-defined direct-pathway MSNs were found to respond to cocaine *in vivo* (Savell et al., 2020), even though all direct-pathway MSNs express both D_1R and NMDAR. It is unknown how much of this *in vivo* variation can be attributed to circuit factors, such as heterogeneity in dopaminergic or glutamatergic inputs to the striatum, *versus* intrinsic properties of striatal MSNs. We therefore sought initially to determine whether the signaling responses of cultured primary striatal neurons show intercellular heterogeneity, by measuring D_1R- and NMDAR-regulated PKA and ERK1/2 signaling in single cells at a large scale.

Genetically-encoded biosensors based on fluorescent or bioluminescent proteins allow biochemical processes to be tracked in living cells with imaging technologies that detect changes in fluorescence or luminescence emitted by one or more tagged proteins. Many such sensors are based on the principle of fluorescence (or Förster) resonance-energy transfer (FRET) and allow endogenous signaling events to be monitored without overexpression of signaling molecules (Miyawaki, 2011). Several studies have used such biosensors to probe endogenous signaling dynamics in striatal neurons, employing a variety of imaging modalities

Molecular Pharmacology Fast Forward. Published on September 9, 2021 as DOI: 10.1124/molpharm.121.000290
This article has not been copyedited and formatted. The final version may differ from this version.

including wide-field and confocal microscopy (Castro et al., 2013; Yapo et al., 2017; Yapo et al., 2018; Mariani et al., 2019; Muntean et al., 2018). Evidence for intercellular response variability can be seen in many of these studies, but with analysis typically restricted to a few dozen cells, intercellular differences were not explored in detail. Here, we performed FRET biosensor imaging using high-content microscopy to rapidly image hundreds or thousands of cells over time, and combined this with immunofluorescence to characterize multiple dimensions of signaling pathway activation.

Using this approach in primary striatal neurons, we explore intercellular variability in PKA and ERK1/2 responses to pharmacological stimulation of D_1Rs or NMDARs, and to direct activation of adenylyl cyclase. Using biosensors localized to either the cytosol or nucleus, we measure compartment-specific signaling in single cells segmented by morphology, in order to identify cell types that exhibit distinct response profiles. Focusing on striatal MSNs we also identify novel interactions between PKA and ERK1/2 signaling that occur in a cell-compartment specific manner.

Materials and Methods

Drugs and Reagents

Unless otherwise noted, products were purchased from Sigma-Aldrich. SKF 81297 hydrobromide (Toronto Research Chemicals), SCH 772984 (Selleckem), forskolin, phorbol-12-myristate-13-acetate (VWR) and U0126 stocks were prepared at 10 μM in DMSO and stored at -80 °C. NMDA was prepared fresh in Hank's balanced salt solution (HBSS) (Wisent). The drug

Molecular Pharmacology Fast Forward. Published on September 9, 2021 as DOI: 10.1124/molpharm.121.000290
This article has not been copyedited and formatted. The final version may differ from this version.

concentrations used in experiments are reported upon the first usage of each drug and remain unchanged for subsequent experiments.

Animals

Sprague-Dawley dams with postnatal day 1 pups were purchased from Charles River, Saint-Constant QC, Canada. Animals were maintained on a 12/12-hour light/dark cycle with free access to food and water. Rats expressing Cre recombinase under the control of the Drd1 promoter (LE-Tg(Drd1a-iCre)3Ottc, Rat Genome Database 10412325) were obtained from the Rat Resource and Research Center (Strain #767, donors Brandon Harvey and Jim Pickel, NIDA/NIMH). All procedures were approved by the McGill University Animal Care Committee, in accordance with Canadian Council on Animal Care guidelines.

Isolation and culture of primary striatal neurons

Primary striatal neurons were prepared from mixed male and female postnatal day 1 pups as previously described (Jones-Tabah et al., 2020). One day in advance, 96-well optical bottom imaging plates (Nunc) were coated overnight with 0.1 mg/ml poly-D-lysine dissolved in phosphate-buffered saline (PBS for cell culture - Sigma). Prior to dissection, plates were washed three times with sterile water and allowed to dry, and all required solutions were warmed to 37 °C. Pups were decapitated and brains were rapidly removed and placed in ice cold HBSS without calcium and magnesium (Wisent). Striata were dissected, and then digested on a rotator at 37 °C for 18 min with papain diluted to a final concentration of 20 units/ml in a neuronal medium (Hibernate A Minus Calcium, BrainBits). Next, in order to halt digestion,

Molecular Pharmacology Fast Forward. Published on September 9, 2021 as DOI: 10.1124/molpharm.121.000290
This article has not been copyedited and formatted. The final version may differ from this version.

tissue was transferred for 2 min to HBSS containing 10% fetal bovine serum, 12 mM $MgSO_4$, and 10 units/ml DNase1 (Roche). Striata were pelleted by centrifugation at 300 X *g* for 5 min and supernatant was removed. Tissue was then triturated in HBSS with 12 mM $MgSO_4$ and 10 units/ml DNase1 using a fire-polished Pasteur pipette. Once a cell suspension was produced (approximately 20 up and down triturations), it was passed through a 40 μm mesh filter (Fisher) to remove undigested tissue and then centrifuged on an OptiPrep™ gradient as previously described (Brewer and Torricelli, 2007), in order to remove cell debris. Purified neurons were then counted and diluted in Neurobasal™-A Medium (NBA) with 1X final concentration of B27 supplement (Gibco), 1% GlutaMAX (Gibco) and 1% penicillin/streptomycin (henceforth referred to as complete NBA) supplemented with 10% fetal bovine serum. On a pre-coated 96-well plate (see above), 50,000 cells were plated in 75 μl volume per well. Sixteen hours after plating, cells were washed with HBSS without calcium and magnesium, and media was changed for complete NBA, containing 5 μM cytosine-D-arabinoside to inhibit glial cell proliferation. Cultures were maintained in complete NBA, and media was refreshed by exchanging 30% of the volume with fresh media every 3 days.

Virus production and transduction of primary neurons

The FRET-based protein kinase biosensors AKAR3-EV and EKAR-EV were generously provided by Dr. Michiyuki Matsuda (Komatsu et al., 2011) and expressed with either nuclear export (NES) or nuclear localization (NLS) peptide sequences. FRET biosensors were expressed using a neuron-specific adeno-associated virus plasmid, pAAV-SynTetOFF (Sohn et al., 2017), kindly provided by Dr. Hiroyuki Hioki. All experiments were performed with AAV serotype 1

Molecular Pharmacology Fast Forward. Published on September 9, 2021 as DOI: 10.1124/molpharm.121.000290
This article has not been copyedited and formatted. The final version may differ from this version.

produced by the Neurophotonics Platform Viral Vector Core at Laval University, Québec. Primary striatal neurons were transduced by adding AAV directly into the culture media three days after cell plating, using a multiplicity of infection of 5000 viral genomes/cell. Neurons were then maintained as described above for 7 days prior to imaging.

High-content FRET imaging in primary neurons

Live-cell imaging was performed at 37°C and with 3% CO_2 using an Opera Phenix™ high-content confocal microscopy system (Perkin Elmer). One hour prior to imaging, media was replaced with 90 μl of HBSS with calcium, magnesium and sodium bicarbonate (Wisent). For antagonist experiments, antagonist or vehicle was also added at the appropriate concentration. Plates were transferred to the Opera Phenix™ and allowed to acclimatize in the live-cell chamber for 10 min before baseline image acquisition. Images were acquired using a 40X water-immersion objective using a 425 nm laser for excitation of CFP. Emissions were detected with filters at 435-515 nm (CFP) and 500-550 nm (YFP). For time-course experiments, approximately 20 fields were imaged per well, with fields being evenly spaced across the well. Baseline images were acquired (Time = 0) and then vehicle or drug solution was added directly to each well at a volume of 10 μl to achieve the required final concentration in the well. Images were then acquired at the indicated intervals. In order to accommodate for imaging delay between sequentially imaged wells of a plate, drugs were added with staggered timing to ensure that images of each well were acquired after the specified time had elapsed. Following each imaging session, cells were fixed and could be processed for immunofluorescence, as described next.

Molecular Pharmacology Fast Forward. Published on September 9, 2021 as DOI: 10.1124/molpharm.121.000290
This article has not been copyedited and formatted. The final version may differ from this version.

Cell fixation and immunofluorescence

Cells were fixed for 10 min in 2% paraformaldehyde prepared in PBS. Fixed cells were then washed twice with PBS and permeabilized for 10 min using 0.3% Triton X-100 in PBS. Blocking was performed for 3 hours at 4°C with 5% bovine serum albumin (BSA) in PBS. Next, cells were incubated overnight at 4°C with primary antibodies diluted in PBS with 5% BSA, then washed twice with PBS, and subsequently incubated for 3 hours at room temperature with secondary antibodies diluted in PBS with 5% BSA. After two additional washes with PBS, cells were incubated with Hoechst dye (Invitrogen) diluted 1:10,000 in PBS. The following primary antibodies and dilutions were used: anti-DARPP-32 (1:1000, catalogue #2302, Cell Signaling Technology), anti-cFos (1:2000, catalogue #sc-52, Lot #C1010, Santa Cruz), anti-phospho-H3-Ser10 (1:1000, catalogue #5176, Abcam), anti-protein kinase A catalytic subunit (1:1000, catalogue #610980, BD Biosciences). Secondary antibodies were Alexa 488 anti-mouse (1:1000; A21236) and Alexa 647 anti-rabbit (1:1000; A21245), both from Invitrogen. Fluorescence imaging of fixed cells was performed in an Opera Phenix™ high-content confocal microscope at 40X magnification.

Image processing and fluorescence quantification

All image analysis was performed using Columbus™ analysis software (Perkin Elmer) using the following generalized workflow. For FRET imaging, transduced cells were automatically identified using “Method B” run on the combined CFP and YFP fluorescence intensity. Specific thresholds for object seize, brightness and contrast were optimized for each

Molecular Pharmacology Fast Forward. Published on September 9, 2021 as DOI: 10.1124/molpharm.121.000290
This article has not been copyedited and formatted. The final version may differ from this version.

sensor and then kept constant for all experiments. The identified objects were then further filtered based on morphology and fluorescence intensity to exclude dead cells, non-cell objects and clusters of overlapping cells. Specific parameters were determined by visual inspection and were adjusted for each sensor. After filtering the object population, CFP and YFP intensities at each pixel were used to calculate the FRET ratio (YFP/CFP), which was then averaged to create a single FRET ratio for each object at each time-point. Values for fluorescence intensities, FRET ratio, object area, object roundness and spatial coordinates within the image were calculated and exported as text files for further analysis. The same pipeline was applied for quantitative immunofluorescence experiments, except that nuclei were first detected using the Hoechst stain so as to create a mask to define a region in which fluorescence signals from the Alexa-488 and Alexa-647 channels were then quantified.

Single cell analysis

For time-course FRET imaging, single cells were tracked across time points using an analysis script written in R (code and sample data are available on the Hébert lab GitHub https://github.com/HebertLab/Single-Cell-FRET, and the complete data set is available upon request). This script was applied to the output of the image analysis. Objects were matched between time-points using the Cartesian coordinates of each object in the image, with a threshold set for maximum acceptable displacement between subsequent images. To ensure correct matching of objects at each time-point, the size and fluorescence intensity of each object was cross-checked, and objects which exhibited a change in size or brightness of greater than 30% were excluded from analysis. Only objects that could be positively matched across all

Molecular Pharmacology Fast Forward. Published on September 9, 2021 as DOI: 10.1124/molpharm.121.000290
This article has not been copyedited and formatted. The final version may differ from this version.

6 time points in the experiment were included for analysis. ΔFRET values were then calculated for each object relative to the object's baseline FRET, and converted into percent changes in FRET (%ΔF/F). Here, the denominator (F) was calculated as the average baseline FRET, not of the particular cell in question, but rather of *all* cells sampled in the same well. This approach avoided extremely high %ΔF/F values that tended to occur with cells having a very low baseline FRET value. The number of cells analyzed in each experiment is indicated in the figure legends.

Values corresponding to single cells from independent experiments were then pooled for data visualization in heat maps. Grouping of FRET responses by either magnitude or kinetics was performed by time-series clustering provided by the TSclust package, in R using the "pam" and "shape" functions for clustering by response magnitude and kinetics, respectively (Montero and Vilar, 2014). All figures were generated as R markdown files. R scripts for analysis and data visualization are available on the Hébert lab GitHub (https://github.com/HebertLab/Single-Cell-FRET).

Response Clustering Analysis

For FRET datasets, response types (e.g. High, Med, Low, None) were assigned based on the time-series clustering described in the previous section. Mean response profiles for each of the defined clusters from Figures 4 and 5 can be seen in Supplemental Figure 2. Mean response profiles for each cluster in Figures 6 and 7 are shown within the respective figures. For immunofluorescence analysis, z scores were calculated for each cell using the fluorescent intensities in the vehicle treated condition as reference population. Responses were then

Molecular Pharmacology Fast Forward. Published on September 9, 2021 as DOI: 10.1124/molpharm.121.000290
This article has not been copyedited and formatted. The final version may differ from this version.

defined as follows: $z < 1$, no response, $1 < z < 2$, low response, $2 < z < 3$, medium response, $z > 3$, high response.

Statistical analysis

All statistical testing was performed in R using the rstatix package, or in GraphPad Prism 9. Data in **Fig. 1** and **Fig. 6** were analyzed using Bonferroni-corrected t-tests, with each treatment being compared to DMSO. In **Fig. 3** and **Fig. 7**, data were analyzed first by 2-way ANOVA, using treatment and cell-type as factors (Fig. 3) or pretreatment and response cluster as factors (Fig. 7). ANOVA was followed by multiple comparisons performed using Bonferroni-corrected t-tests, with significant results indicated. All statistical comparisons were performed using the mean and variability of biological replicates (as opposed to individual cells), where a biological replicate was defined by cells isolated from a distinct group of rats i.e. cells isolated from a partial or entire litter of pups. Curve fitting was performed in GraphPad Prism 9 using the Logistic equation for sigmoidal curves, and the Rise-and-fall time-response equation from the Pharmechanics package for rise to steady state curves (Hoare et al., 2020).

Results

In the experiment presented in **Fig. 1**, we expressed substrate-based reporters of PKA (AKAR) and ERK1/2 (EKAR) activity with either nuclear export (NES) or nuclear localization (NLS) sequences in primary striatal neurons and then performed live-cell high-content imaging (**Fig. 1A, D, respectively**). Neuronal cultures were treated with either vehicle, SKF 81297 (a selective agonist of D1-like receptors, presented in figures as SKF), NMDA, a combination of these two

Molecular Pharmacology Fast Forward. Published on September 9, 2021 as DOI: 10.1124/molpharm.121.000290
This article has not been copyedited and formatted. The final version may differ from this version.

drugs, or forskolin (a direct activator of adenylyl cyclase, presented in figures as FSK). Images were acquired before treatment, and again 10 min after stimulation and the FRET changes of individual cells (shown as violin plots) and biological replicates (points) are shown (**Fig. 1B-C, Fig. 1E-F**). Broadly, we observed activation of cytosolic and nuclear PKA and ERK1/2 by all drug conditions, with the exception that NMDA activated nuclear, but not cytosolic PKA.

Focusing on nuclear-localized (NLS) biosensors, we next explored the use of morphological criteria in our analysis to explore the intercellular variability of nuclear FRET responses. We first compared the size and roundness of transduced nuclei to the basal FRET ratio of each cell (calculated as above); basal FRET ratios were found to be variable, ranging from 0.5 to 1.25, but evenly distributed across cells with varying size and roundness (**Fig. 2A, D**). Published evidence suggests that MSNs can be distinguished from other striatal cell types based on a distinctive nuclear morphology (Matamales et al., 2009). Accordingly, we hypothesized that cells with 50-100 μm^2 round nuclei (roundness score >0.9) (**Fig. 2A, D** purple squares) would be enriched for MSNs. The cut-offs for defining these cells, which we refer to as "medium-round", were based on the previous finding that striatal MSNs *in vivo* were found to have highly round nuclei, with cross-sectional area of 75-95 μm^2 (Matamales et al., 2009). We also assigned the remaining cells to three additional categories based on their nuclear morphology **(Fig. 2A, D** coloured boxes). We next compared the FRET response of each cell plotted against the CFP intensity (a surrogate measure for the expression level of the biosensor) and observed that while FRET responses appeared independent of expression level, cells with this "medium round" morphology tended to exhibit higher biosensor expression and larger

Molecular Pharmacology Fast Forward. Published on September 9, 2021 as DOI: 10.1124/molpharm.121.000290
This article has not been copyedited and formatted. The final version may differ from this version.

FRET responses compared to the other categories of cell. (**Fig. 2B, E**). Within these "medium round" cells there appeared to be no overall association between the expression level of the biosensor and the response magnitude to stimulation (**Fig. 2 C, F**). However, for the EKAR biosensor specifically, we did observe a qualitative reduction in the number of high-responses among cells with the highest biosensor expression levels (**Fig. 2F)**. While no corrective action was taken in our analysis, it does raise the possibility that when expression levels are too high, biosensor responses may be blunted due to presence of unphosphorylated "spare biosensors". Overall, we concluded that the observed differences in biosensor expression level do not account for differences in response magnitude.

To further explore our hypothesis that the "medium round" cell group was enriched in striatal MSNs we performed immunofluorescence to measure the striatal cell marker DARPP-32 (Ivkovic and Ehrlich, 1999) and used Hoechst dye to stain nuclei and determine nuclear morphology (**Fig. 3A**). We plotted relative DARPP-32 expression levels on a coordinate plot of nuclear size and roundness, and found that as predicted, cells with high levels of DARPP-32 expression were concentrated in the "medium round" cell grouping (**Fig. 3B**). Specifically, out of 34,429 cells imaged, 12,815 had high DARPP-32 expression, (defined by a z-score > 0), and of those, 12,296 (or 95.9%) were found in the "medium round" grouping. To confirm the enrichment of D_1R expressing MSNs in the "medium round" cell group, we cultured striatal neurons from rats expressing Cre-recombinase under the control of the Drd1 promoter, and transduced these with a Cre-dependent mCherry-expressing AAV (**Fig. S1A**). When we again

Molecular Pharmacology Fast Forward. Published on September 9, 2021 as DOI: 10.1124/molpharm.121.000290
This article has not been copyedited and formatted. The final version may differ from this version.

quantified nuclear morphology we found that mCherry-positive neurons were concentrated in the “medium round” grouping (**Fig. S1B**).

Re-analysis of the FRET data presented in **Fig. 1** by segregating cells into these nuclear morphology-defined groups showed that, for both nuclear PKA (AKAR-NLS) and nuclear ERK1/2 (EKAR-NLS), the response to drug treatments significantly differed between cell-types (2-way ANOVA, Treatment x Cell-Type interaction, $p<0.0001$ and $p<0.001$, for AKAR-NLS and EKAR-NLS respectively)(**Fig. 3C, D**). Specifically, “medium round” cells were more responsive to all drugs with respect to both PKA and ERK1/2 signaling, with several individual comparisons being statistically significant. Finally, as an independent method of verifying these differences in drug response, we performed cFos immunofluorescence on striatal cultures after 3-hour drug exposure (**Fig. 3E**). Here we again found that cFos induction significantly differed between cell types (2-way ANOVA, Treatment x Cell-Type interaction $p<0.0001$) and that relative to all other cell groups, “medium round” cells were significantly more responsive in regards to cFos induction by SKF 81297, NMDA and forskolin.

Using this morphological approach to focus our analysis on the MSN-enriched cells defined by “medium round” nuclear morphology, we next investigated the intercellular variability in nuclear PKA and ERK1/2 signaling. Single cell analysis allowed us to visualize the responses of individual cells, imaged at 10-min intervals for 50 min after stimulation (**Fig. 4A-B**). In order to group cell with similar responses, we performed time-series clustering (see *Materials and Methods*) to assign each cell to a specific response-type based on the magnitude

Molecular Pharmacology Fast Forward. Published on September 9, 2021 as DOI: 10.1124/molpharm.121.000290
This article has not been copyedited and formatted. The final version may differ from this version.

of FRET response. Clustering was performed independent of biological replicate or treatment condition. Categories were subsequently labelled as non-responsive cells, low, medium and high responding cells, based on the response profile of the cluster (**Fig. S2**). We then analyzed drug responses both in terms of the average percentage of cells in each replicate displaying a given response type (**Fig. 4C-D**) and by the average response magnitudes, either when all cells were included, or when cells in the non-responsive cluster were excluded (**Fig. 4E-F**). This analysis revealed that although the D_1R agonist SKF 81297 initially appeared to be the weakest activator of nuclear PKA and ERK1/2, this impression was driven by a lower percentage of responding cells, not by a lower average magnitude of response per cell (**Fig. 4E-F**). Importantly, the rank-order of drug effects differed, depending on whether analysis was restricted to drug-responsive cells or if cells that were unresponsive to drug were included (**Fig. 4E-F**).

We also performed a similar single cell analysis of PKA and ERK1/2 signaling in the *cytosol*, using biosensors fused to a nuclear export sequence (NES) (**Fig. 5A-F**). Whereas in the case of NLS-tagged biosensors, the nuclear morphology was used to filter cells and enrich for MSNs, in the analysis of NES-tagged biosensors, this segmentation was not possible, and so the total population of imaged cells was analyzed. Cytosolic signaling responses largely paralleled those in the nucleus, with three notable differences. First, while NMDA activated nuclear PKA (**Fig 4A)**, it had a minimal effect on cytosolic PKA (**Fig. 5A)**. Second, when only responding cells were considered, SKF 81297 was as efficacious as forskolin in activating nuclear PKA (**Fig. 4E-F)** but less efficacious than forskolin in activating cytosolic PKA (**Fig. 5E)**. Lastly, whereas nuclear responses were almost exclusively stimulatory (i.e. increased FRET) and responses to vehicle

Molecular Pharmacology Fast Forward. Published on September 9, 2021 as DOI: 10.1124/molpharm.121.000290
This article has not been copyedited and formatted. The final version may differ from this version.

were minimal, in the cytosol we observed more pronounced inhibitory responses to ligand stimulation and larger vehicle responses, both in the positive and negative direction.

The rapid and sustained activation of nuclear PKA by D_1R agonists in rat striatal neurons which we observed (**Fig. 4A,E**) has been previously described in mouse brain slices (Yapo et al., 2018). In cultured striatal neurons, nuclear ERK1/2 was also activated to a similar, if not greater, degree by stimulation of either the D_1R or adenylyl cyclase (**Fig. 4B,F**). Although the strong and rapid activation of nuclear PKA would suggest a potentially important functional role in this structure, the specific nuclear targets of PKA in striatal neurons remain largely uncharacterized. To investigate the relative contributions of PKA and ERK1/2 to the regulation of specific nuclear signaling events, we utilized two inhibitors of ERK1/2-dependent signaling: U0126, an inhibitor of the upstream protein kinase MEK, and SCH772984, an inhibitor of ERK1/2. Pretreatment with either inhibitor abolished nuclear ERK1/2 signaling in response to SKF 81297 or forskolin (**Fig. 6A)**. Similar results were obtained for cFos expression, except that the inhibitors did not fully inhibit the response to forskolin (**Fig. 6B**). At the single-cell level, reduction in cFos immunofluorescence were evident both in terms of maximum levels of induction, and the percentage of responding cells, but with forskolin treatment, some cFos induction was again still evident (**Fig. S3A,B**). We next examined phosphorylation of histone H3 on serine 10 (pH3-S10), a transcription-activating event that has been associated with D_1R-dependent ERK1/2 signaling in striatal neurons *in vivo* (Bertran-Gonzalez et al., 2008; Brami-Cherrier et al., 2005). Here, pH3-S10 was largely unaffected by either inhibitor, with a partial but statistically non-significant reduction observed only for SCH772984 (**Fig. 6C, Fig. S3C,D**). This suggests a role for

Molecular Pharmacology Fast Forward. Published on September 9, 2021 as DOI: 10.1124/molpharm.121.000290
This article has not been copyedited and formatted. The final version may differ from this version.

PKA-dependent, and ERK1/2-independent signaling in the deposition of pH3-S10 in primary striatal neurons.

Although to our knowledge neither U0126 or SCH772984 are known to have off-target effects on PKA, we nonetheless measured PKA-dependent signaling to confirm that it was preserved in the presence of these inhibitors. Unexpectedly, we observed that the ERK1/2 inhibitor reduced nuclear, but not cytosolic PKA activation after a 10-min treatment with SKF 81297 or forskolin (**Fig. 6D,E**). This decrease was transient, and levels of nuclear PKA activation similar to that observed in vehicle pretreated cells were still achieved in the presence of either inhibitor 20-50 min after stimulation (**Fig. S4**). To investigate the altered kinetics of nuclear PKA activation, single-cell responses were subjected to kinetic clustering analysis (see *Materials and Methods*), in order to categorize cells according to the time-course of their responses to drug. This analysis revealed four predominant response types (**Fig. 6F**). Both inhibitors tended to increase the percentage of "slow" responding cells at the expense of "fast" responding cells, but these changes did not reach statistical significance (**Fig. 6G**).

We next performed high-content imaging on a shorter timescale (1-min intervals from 1-9 min) to more precisely characterize the timing of early cytosolic and nuclear signaling events. Stimulation with either SKF 81297 or forskolin rapidly activated cytosolic PKA, which reached maximum amplitude within 60 s, while the onset of nuclear PKA activity was slower, peaking 6-7 min after stimulation with either SKF 81297 or forskolin (**Fig. 7A,B**). The time course of nuclear PKA activation in primary striatal neurons appeared sigmoidal, similar to previous

Molecular Pharmacology Fast Forward. Published on September 9, 2021 as DOI: 10.1124/molpharm.121.000290
This article has not been copyedited and formatted. The final version may differ from this version.

findings in mouse brain sections (Yapo et al., 2018). Neither U0126 or SCH772984 detectably altered cytosolic PKA activity when measured on this shorter time-scale (**Fig. 7C,D**) but significant differences were found in the extent of nuclear PKA activation (2-way ANOVA, Pretreatment x Time interaction, $p<0.0001$ for both SKF and FSK) (**Fig. 7E,F**) with either inhibitor appearing to reduce nuclear PKA. Nuclear ERK1/2 activation followed similar kinetics to that of nuclear PKA, reaching its maximum 5-6 min after SKF 81297 or forskolin treatment, and as expected, was abolished by pretreatment with the two inhibitors of ERK1/2-dependent signaling, U0126 or SCH772984 (**Fig. 7G,H**). Response-magnitude clustering (**Fig. 7I**) revealed that within this 10-min time frame, U0126 and SCH772984 did not affect the percentage of non-responsive, or low-responsive cells, but significantly reduced the number of high responding cells to either SKF 81297 or forskolin (**Fig. 7J,K**). In the case of forskolin, this was matched by a significant increase in cells with medium response magnitude (**Fig. 7K**). Taken together, these findings suggest that ERK1/2 plays a facilitatory role in the activation of nuclear PKA and that so called “high-responders” at the level of nuclear PKA exhibit the greatest sensitivity to inhibition of the ERK1/2 pathway.

A potential mechanism that could explain the reductions in nuclear, but not cytosolic, PKA signaling would be ERK1/2-dependent facilitation of PKA nuclear translocation. To measure nuclear translocation of PKA, we used immunofluorescent detection of the catalytic subunit of PKA (PKA_C) and used Hoechst dye to demarcate the nuclear compartment. Prior to stimulation, PKA_C was largely absent from the nucleus but its levels were increased upon stimulation with SKF 81297 or forskolin (**Fig. 8A,B**). This nuclear localization of PKA_C was apparent only in a

Molecular Pharmacology Fast Forward. Published on September 9, 2021 as DOI: 10.1124/molpharm.121.000290
This article has not been copyedited and formatted. The final version may differ from this version.

subset of cells (approximately 25% and 45% of putative MSNs for SKF 81297 and forskolin, respectively) (**Fig. 8C, Fig. S5**). Pretreatment with U0126 or SCH772984 did not alter the translocation of PKA_C to the nucleus (**Fig. 8D,E, Fig. S5A,B**) indicating that ERK1/2 inhibition does not attenuate nuclear PKA signaling by reducing nuclear accumulation of PKA_C.

The finding that U0126 and SCH772984 did not affect the movement of PKA_C to the nucleus would instead suggest that ERK1/2 promotes the relative activity PKA without altering the quantity of PKA in the nucleus. To test this hypothesis, we sought to determine whether co-activation of ERK1/2 signaling through an independent pathway could enhance nuclear PKA activation stimulated by forskolin. In the striatum *in vivo,* independent activation of PKA and ERK1/2 signaling could potentially occur via co-activation of D_1R and NMDARs. However, since we had previously observed that NMDA can independently activate nuclear PKA signaling (**Fig. 4**) we opted to use phorbol 12-myristate 13-acetate (PMA) to activate ERK1/2 signaling via protein kinase C (PKC) (Castagna et al., 1982). As expected, PMA or forskolin activated nuclear ERK1/2 (**Fig. 9A, Fig. S6A**). Compared to treatment with either drug alone, co-treatment with forskolin and PMA resulted in a faster onset, but produced similar maximum levels of ERK1/2 activity in the nucleus, and SCH772984 abolished the signal (**Fig. 9A, Fig. S6A**). PMA activated nuclear PKA to a similar degree as forskolin, both in terms of mean response and percentage of responding cells (**Fig. 9B, Fig. S6B**). This effect was initially unexpected given the pharmacology of PMA, but activation of PKA through a PKC-dependent mechanism has previously been described to occur in neurons (Chen et al., 2017). We further found that nuclear PKA activation by PMA was abolished by SCH772984, suggesting that this effect was ERK1/2-dependent and

Molecular Pharmacology Fast Forward. Published on September 9, 2021 as DOI: 10.1124/molpharm.121.000290
This article has not been copyedited and formatted. The final version may differ from this version.

not directly mediated by PKC. Compared to treatment with either drug alone, the combination of PMA and forskolin increased the rate of nuclear PKA activation, and similar to our previous observations, this was attenuated by SCH772984 (**Fig. 9B, Fig. S6B**). PMA also activated cytosolic PKA (**Fig. 9C, Fig. S6C**), but this cytosolic response differed from the nuclear response in three respects: it occurred more promptly, it was smaller, and it was not clearly inhibited by SCH772984 (compare **Fig. 9B *vs.* 9C**). Taken together, findings further argue for nuclear-specific cross-talk whereby ERK1/2 activation can promote PKA signaling in striatal neurons.

Discussion

Cells are often categorized by anatomical location, morphological features, functional properties, or the expression of specific molecular markers. Cell type designations are inherently limited by the availability of technologies used to isolate, sort or label cells. As technologies have become available for single-cell profiling at the genomic, proteomic, and functional levels, previously inaccessible heterogeneity has been revealed within cell populations that were once treated, out of necessity, as homogenous (Cadwell et al., 2016; Fuzik et al., 2016). This "homogeneity assumption" has also affected the study of cellular signaling and molecular pharmacology. For example, drug effects are often expressed in terms of a single *averaged* drug response determined from a population of interest, but biologically important differences may exist in the way drugs engage individual cells within such a population. Importantly, some generalization allows us to conceptualize complex systems such as signaling pathways and the way drugs act on them. However, this simplification also arises from limitations in the available technology. Recently, new techniques including high-content

Molecular Pharmacology Fast Forward. Published on September 9, 2021 as DOI: 10.1124/molpharm.121.000290
This article has not been copyedited and formatted. The final version may differ from this version.

imaging have allowed researchers to investigate the existence and importance of intercellular heterogeneity in signaling pathway engagement (Handly, Yao, and Wollman, 2016; Singh et al., 2010; Yao, Pilko, and Wollman, 2016; Bao et al., 2010; Tsou et al., 2011; Chavez-Abiega et al., 2021). Here, we illustrate a simple approach in which the combination of biosensors and high-content microscopy allowed us to capture the signaling dynamics of thousands of primary cells in culture.

The single-cell approach reported here offers at least one major advantage and limitation. The main advantage is throughput. The ability to image thousands of cells decreases experimenter bias and increases replicability. These large datasets also allow us to consider the *proportion* of responding cells when investigating drug effects. As an example, seemingly identical results could be produced by a few strongly responding cells or many weakly responding cells. A case in point is the activation of nuclear PKA by D_1R *vs.* NMDAR agonists. In the aggregate response, the two drugs appeared to produce similar effects (**Fig 1H**); the single-cell results disambiguated this observation, revealing that while NMDA activates nuclear PKA in a larger proportion of cells, the D_1R agonist produces larger responses. The main limitation of our single-cell approach is the lack of temporal control of drug release within the high-content imaging system. For this reason, this approach would not be useful for studying cellular responses to transient receptor stimulation.

This approach applied to striatal neurons yielded three main sets of findings. First, we uncovered substantial intercellular variability in the magnitude and kinetics of signaling

Molecular Pharmacology Fast Forward. Published on September 9, 2021 as DOI: 10.1124/molpharm.121.000290
This article has not been copyedited and formatted. The final version may differ from this version.

pathway activation in response to various pharmacological stimuli. Second, as well as confirming a previous report that D_1R activation in striatal neurons rapidly activates both nuclear and cytosolic PKA (Yapo et al., 2018), we showed that ERK1/2 is also rapidly and persistently activated in the nucleus of primary striatal neurons; moreover, nuclear PKA and ERK1/2 activation were induced not only by D_1R agonist but also by NMDAR agonists, cAMP signaling, and by an activator of PKC. These findings indicate that many distinct pathways converge on these nuclear signals. Finally, we describe a novel mode of cross-talk between PKA and ERK1/2, whereby ERK1/2 signaling regulates the activity of PKA specifically in the nucleus.

The molecular features that give rise to the signaling heterogeneity observed in our experiments remain to be determined, but could potentially arise from differences in receptor density, or the regulation of intracellular signaling cascades. Since our striatal cultures were unlikely to comprise pure populations of striatal MSNs, we used nuclear morphology measurements in order to refine the population of analyzed cells to include only those cells most likely to be MSNs. Within this MSN-enriched population, the D_1R agonist SKF 81297 elicited nuclear PKA and ERK1/2 responses in ~30% and ~40% of cells respectively. If one assumes that most “medium round” cells were in fact MSNs, with around 50% of those MSNs expressing D_1Rs as reported *in vivo* (Schambra et al., 1994; Thibault et al., 2013), then our results suggest that most of the cultured D_1R-expressing MSNs responded to the D1 agonist, albeit with widely differing response magnitudes. Even forskolin, which directly activates adenylyl cyclase and is commonly used as a positive control in studies of GPCR-mediated cAMP signaling, produced a range of effect sizes, with approximately 10% of neurons unresponsive to

Molecular Pharmacology Fast Forward. Published on September 9, 2021 as DOI: 10.1124/molpharm.121.000290
This article has not been copyedited and formatted. The final version may differ from this version.

forskolin within the timeframe measured. Importantly, the response magnitude in individual cells was unrelated to the expression level of the biosensor.

Compared to other neurons, striatal MSNs reportedly exhibit larger fluxes in cAMP and PKA signaling in both the cytosol (Castro et al., 2013; Yapo et al., 2017) and nucleus (Yapo et al., 2018). The mechanisms of GPCR-mediated protein kinase signaling to the nucleus have not been fully elucidated, and as argued below, are likely cell-type specific. Although the activated PKA catalytic subunit can enter the nucleus by passive diffusion from the cytoplasm (Harootunian et al., 1993), the inactive PKA holoenzyme has also been observed in the nucleus in neurons (Ilouz et al., 2017). In a previous report, D_1R-dependent nuclear PKA activation in cortical neurons followed slow linear kinetics, consistent with passive diffusion from the cytosol, whereas in striatal neurons, activation of nuclear PKA was rapid, yet with a consistent delay relative to activation of cytosolic PKA (Yapo et al., 2018). Our results largely confirm these previous findings. The ~5-minute delay in nuclear relative to cytosolic PKA activation would be inconsistent with free diffusion of cytosolic cAMP to activate PKA pre-existing in the nucleus. It was previously suggested that activated PKA could facilitate its own entry into the nucleus (Yapo et al., 2018). Our findings suggest that, independent of any effect on the nuclear translocation of PKA, ERK1/2 activation also contributes to enhancing nuclear PKA signaling in striatal neurons.

ERK1/2 has been described as a coincidence detector, synergistically responding to combined D_1R and NMDAR signaling (Valjent et al., 2005). We found that ERK1/2 signaling was

Molecular Pharmacology Fast Forward. Published on September 9, 2021 as DOI: 10.1124/molpharm.121.000290
This article has not been copyedited and formatted. The final version may differ from this version.

stimulated by individual application of the D_1R or NMDAR agonists, with effects occurring in both the cytosol and nucleus. However, in contrast to previous work, the D_1R and NMDAR agonists in combination produced a *sub-additive* effect. These findings may be best explained by two factors: first, our primary striatal cultures were effectively dopamine-free, given that the striatal dopaminergic innervation is entirely extrinsic, and second, *in vivo* striatal dopamine depletion enhances coupling between D_1R and ERK1/2 (Darmopil et al., 2009; Gerfen et al., 2002; Pavón et al., 2006; Santini et al., 2009; Westin et al., 2007). The lack of dopaminergic innervation could thus feasibly explain the potent ERK1/2 activation by D_1R seen in our primary cultures. Furthermore, the activation of cytosolic and nuclear ERK1/2 in nearly all forskolin-stimulated striatal neurons suggest that in these cells, the cAMP cascade is strongly coupled to MAPK activation.

Our data also describe two novel features of nuclear signal transduction in striatal neurons. Firstly, our findings argue against previous studies that have indicated ERK1/2 activity is required for the induction of histone 3 phosphorylation (pH3-S10) in striatal MSNs (Bertran-Gonzalez et al., 2008; Brami-Cherrier et al., 2005). Thus, in our primary striatal cultures, stimulation of D_1R or AC produced strong pH3-S10 induction even under conditions where no ERK1/2 signaling was detected.

We also observed that ERK1/2 signaling contributes to the activation of nuclear PKA. Notably, in striatal neurons stimulated with D_1R agonist or forskolin, nuclear PKA and ERK1/2 were activated with comparable kinetics, and when ERK1/2 signaling was blocked, the rate of

Molecular Pharmacology Fast Forward. Published on September 9, 2021 as DOI: 10.1124/molpharm.121.000290
This article has not been copyedited and formatted. The final version may differ from this version.

nuclear PKA activation was significantly diminished. Moreover, we found that independently promoting ERK1/2 signaling through the PKC pathway could also activate nuclear PKA. This novel mode of cross-talk could contribute to the previously described synergistic effects of co-incident D_1R and NMDA signaling *in vivo*, particularly with respect to the regulation of nuclear functions such as transcription and the epigenetic modifications that regulate it. Although the underlying mechanism remains to be determined, our findings argue that ERK1/2 does not regulate the translocation of PKA to the nucleus, but rather the balance of PKA activity in the nucleus. Given that AKAR is a substrate-based reporter, such an effect could occur through facilitation of PKA activation, or inhibition of phosphatases that normally antagonize PKA-dependent phosphorylation; the specific ERK1/2 substrates mediating this effect remain to be investigated. It is well established that D_1R dependent signalling can promote ERK1/2 activation through multiple routes within striatal MSNs, including via cAMP/PKA/DARPP-32 dependent mechanisms (Paul et al., 2000; Saxena et al., 1999; Valjent et al., 2005) and the numerous points of interaction between these signaling cascades complicates the functional delineation of individual signalling pathways.

Here, we have used high-content microscopy and FRET biosensors to characterize PKA and ERK1/2 signaling in the cytoplasm and nucleus of cultured striatal neurons, and to identify intercellular differences, in both the magnitude and kinetics of signaling responses to drug application. This approach has yielded new observations about the signaling of PKA and ERK1/2 in striatal neurons, and more generally can provide a novel vantage point from which to capture the intercellular nuances of cellular signaling dynamics.

Molecular Pharmacology Fast Forward. Published on September 9, 2021 as DOI: 10.1124/molpharm.121.000290
This article has not been copyedited and formatted. The final version may differ from this version.

Declaration of Competing Interest

The authors declare that they have no known competing financial interest or personal relationships that could have influenced the work reported here.

Acknowledgements

This work was supported by grants from the Weston Brain Institute [RR181011] and Canadian Institutes of Health Research [PJT-256524]. J.J.T was supported by doctoral studentships from the Canadian Institutes of Health Research and the McGill Healthy Brains for Healthy Lives initiative. R.M. was supported by studentships from the McGill-CIHR Drug Development Training Program and the McGill Faculty of Medicine. We thank Dr. Michiyuki Matsuda (Kyoto University) for providing us with biosensor constructs and Dr. Hiroyuki Hioki (Kyoto University) for providing AAV plasmids. T.E.H. is the holder of the Canadian Pacific Chair in Biotechnology. We thank the McGill Pharmacology and Therapeutics Imaging and Molecular Biology platform, as well as the McGill Advanced BioImaging facility for training and assistance with microscopy and image analysis. We thank Hanan Mohammad for help in colony management for the Drd1-Cre transgenic rats, and Emma Paulus for assistance in maintaining neuronal cultures. Lastly, we thank members of the Hébert, Clarke and Tanny labs for feedback and guidance throughout the development of the project, and for critical reading of the manuscript.

Molecular Pharmacology Fast Forward. Published on September 9, 2021 as DOI: 10.1124/molpharm.121.000290
This article has not been copyedited and formatted. The final version may differ from this version.

Author Contributions.

Participated in research design: **Jones-Tabah, Tanny, Clarke, Hébert**

Conducted experiments: **Jones-Tabah, Martin**

Contributed new reagents or analytic tools: **Martin**

Performed data analysis: **Jones-Tabah, Tanny, Martin, Clarke, Hébert**

Wrote or contributed to the writing of the manuscript: **Jones-Tabah, Tanny, Clarke, Hébert**

Figure Legends

Figure 1: High-content imaging of nuclear PKA and ERK1/2 activity with FRET biosensors A) Representative image of striatal neurons expressing a FRET reporter tagged with a nuclear export signal (NES) (top) and outlines showing object identification by Columbus software. B, C) Percent change in FRET ratio (%ΔF/F) 10 min after drug stimulation. Violin plots show the range of *individual* cell responses, while points indicate the mean of each *biological replicate*. D) Representative image of primary striatal neurons expressing a FRET reporter tagged with nuclear localization signal (NLS) (top) and outlines showing object identification by Columbus software E, F) Percent change in FRET ratio (%ΔF/F) 10 min after drug stimulation. Violin plots show the range of *individual* cell responses, while points indicate the mean of each *biological replicate*. Experiments comprised 8 (AKAR-NES, EKAR-NES and EKAR-NLS) or 10 (AKAR-NLS) biological replicates collectively containing 3,166, 7,186, 3,620, and 3,740 cells, respectively. Statistical comparisons were performed on biological replicates by Bonferroni corrected t-tests comparing each treatment to DMSO vehicle. *p<0.05, **p<0.01, ***p<0.001, ****p<0.0001.

Molecular Pharmacology Fast Forward. Published on September 9, 2021 as DOI: 10.1124/molpharm.121.000290
This article has not been copyedited and formatted. The final version may differ from this version.

Abbreviations and drug concentrations: DMSO, dimethyl-sulfoxide; SKF, SKF 81297 (1 µM); NMDA, N-methyl-D-aspartic acid (5 µM); and FSK, forskolin (5 µM).

Figure 2: Assessing basal FRET ratios, cellular morphology, FRET responses and biosensor expression levels A,D) Baseline FRET ratio (point color) of single cells, as a function of nuclear size and shape (i.e. cross-sectional area and roundness, respectively). Based on nuclear size and shape, cells were individually assigned to one of four categories, framed by rectangles of different colours (Large elongated- red, Large round- green, Medium elongated- blue and Medium round- purple). B,E) Relationship between FRET response (%ΔF/F) and biosensor expression level (CFP intensity, arbitrary units) across morphology-defined cell types. C,F) Relationship between FRET response (%ΔF/F) and biosensor expression level (CFP intensity, arbitrary units) within "medium round" cells. Colors indicate the four response clusters (i.e. none, low, medium, and high, as described in methods). For all panels, data are merged from all treatment conditions.

Figure 3: Comparison of cellular and signaling phenotypes of nuclear morphology-defined cell types. A) Immunofluorescent labelling of primary striatal neurons for DARPP-32 with Hoechst staining. B) Expression level z-score of DARPP-32 (sectors coded by colour) in single cells plotted on a coordinate map depicting measurements of nuclear size and shape. C) Nuclear PKA activation 10 min after indicated drug treatments. D) Nuclear ERK1/2 activation 10 min after indicated drug treatments. Violin plots represent single cell distribution while open circles represent biological replicates, and black triangles represent the overall mean. E) Induction of

Molecular Pharmacology Fast Forward. Published on September 9, 2021 as DOI: 10.1124/molpharm.121.000290
This article has not been copyedited and formatted. The final version may differ from this version.

cFos, 3 hours after the start of drug treatments. Statistical comparisons were performed by 2-way ANOVA followed by Bonferroni corrected t-tests comparing “medium round” cells to all other cell types for each treatment. *p<0.05, **p<0.01, ***p<0.001, ****p<0.0001 versus “medium round” cells. Experiments consisted of 3 (DARPP-32), 10 (AKAR-NLS) and 8 (EKAR-NLS) biological replicates collectively containing 34,429, 3,620 and 3,740 cells respectively. cFos immunofluorescence was performed on the cells used in all AKAR-NLS and EKAR-NLS FRET experiments and this experiment collectively contains 108,434 cells from 18 biological replicates.

Figure 4: Nuclear PKA and ERK1/2 signaling in single neurons. A, B) Heat maps depicting %ΔF/F of individual cell nuclei imaged at 10-min intervals. Cells are organized into the four response clusters visualized in the following panels. C, D) Percentage of cells falling into each of four response clusters (mean of biological replicates). E, F) Comparison of the mean %ΔF/F time-course for each drug when all cells are included (left) or after removal of non-responding cells (“None” cluster) (right). Shaded region shows the SEM calculated across cells. Experiments consisted of 10 (AKAR-NLS) and 8 (EKAR-NLS) biological replicates collectively containing 1,756 and 2,904 “medium round” cells respectively.

Figure 5: Cytosolic PKA and ERK1/2 signaling in single neurons. A, B) Heat maps depicting %ΔF/F of individual cells imaged at 10-min intervals. Cells are organized into four response clusters as visualized in the following panels. C, D) Percentage of cells falling into each response cluster (mean of biological replicates). E, F) Comparison of the mean %ΔF/F time-course for

Molecular Pharmacology Fast Forward. Published on September 9, 2021 as DOI: 10.1124/molpharm.121.000290
This article has not been copyedited and formatted. The final version may differ from this version.

each drug when all cells are included (left) or after removal of non-responding cells ("None" and "Decrease" clusters) (right). Shaded region shows the SEM calculated across cells. Experiments consisted of 8 biological replicates collectively containing 2,256 (AKAR) and 5,006 (EKAR) cells.

Figure 6: Effect of ERK1/2 inhibition on nuclear responses in striatal neurons. A) Percent change in FRET ratio (%ΔF/F) for EKAR-NLS 10 min after stimulation of cells with vehicle, SKF 81297 or forskolin, in the presence of the MEK inhibitor U0126 (1 μM), ERK1/2 inhibitor SCH772984 (10 nM), or vehicle (DMSO). B) cFos expression 3 hours after the indicated treatment/pretreatment C) H3 phosphorylation on Ser10 (pH3-S10) 60 min after the indicated treatment/pretreatments D) Percent change in FRET ratio for AKAR-NLS 10 min after stimulation. E) Percent change in FRET ratio for AKAR-NES 10 min after stimulation. F) Mean ± SEM response of cells in 4 kinetically defined clusters. G) Percentage of cells falling into each response category across treatment combinations. Experiments consisted of 4 (EKAR-NLS), 18 (cFos), 6 (pH3-S10), 8 (AKAR-NLS) and 6 (AKAR-NES) biological replicates collectively containing 1,354, 212,670, 65,451, 9,712, and 2,887 cells respectively. For all experiments except AKAR-NES, only medium-round nuclei were included in the analysis. Statistical comparisons were performed by 2-way ANOVA followed by Bonferroni corrected t-tests comparing each antagonist to DMSO vehicle within a given treatment condition. #$p<0.05$, ##$p<0.01$ relative to DMSO pretreatment.

Molecular Pharmacology Fast Forward. Published on September 9, 2021 as DOI: 10.1124/molpharm.121.000290
This article has not been copyedited and formatted. The final version may differ from this version.

Figure 7: ERK1/2 inhibition attenuates nuclear PKA activation in striatal neurons. A,B) Time-course of nuclear and cytosolic PKA activation in striatal neurons stimulated with SKF 81297 (A) or forskolin (B). C,D) Cytosolic PKA activation in striatal neurons pretreated with vehicle, U0126, or SCH772984 and stimulated with SKF 81297 (C) or forskolin (D). E,F) Nuclear PKA activation in striatal neurons, pretreated with the indicated inhibitors and stimulated with SKF 81297 (E) or forskolin (F). G,H) Nuclear ERK1/2 activation, otherwise as in panels E and F. I) Mean response profiles of 4 cell groups identified by time-series clustering. J,K) The effect of U0126 or SCH772984 on the mean percentage of cells exhibiting different degrees of nuclear PKA activation in response to SKF 81297 (J) or forskolin (K). Experiments consisted of 6 (AKAR-NES), 20 (AKAR-NLS) and 20 (EKAR-NLS) biological replicates collectively containing 2,887, 10,656 and 9,037 cells respectively. For all experiments except those using AKAR-NES, only medium-round nuclei were included in the analysis. Statistical comparisons (panels J and K) were performed by 2-way ANOVA followed by Bonferroni corrected t-tests comparing each antagonist to DMSO pretreatment within a given treatment condition. *p<0.05, ****p<0.0001.

Figure 8: Nuclear translocation of PKA is induced by D1R or cAMP activation, but does not require ERK1/2 signaling. A) Representative confocal images of the protein kinase A catalytic subunit (PKA_C) in untreated (left) and forskolin stimulated (right) striatal neurons. B) Fluorescent intensity of PKA_C in the nuclear compartment (defined by Hoechst staining), expressed as the percent difference relative to unstimulated cells. C) Frequency histogram showing relative proportion of cells with the indicated levels of nuclear PKA_C fluorescent signal (arbitrary units) 30 min after the indicated treatments. D,E) Effect of vehicle, U0126 (1 μM), or

Molecular Pharmacology Fast Forward. Published on September 9, 2021 as DOI: 10.1124/molpharm.121.000290
This article has not been copyedited and formatted. The final version may differ from this version.

SCH772984 (10 nM) pretreatment on nuclear PKA_C translocation following stimulation with SKF 81297 (D) or forskolin (E). Experiments consisted of 4 (panel B,C) and 6 (panel D,E) biological replicates collectively containing 34,256 and 99,592 cells respectively.

Figure 9: Activation of ERK1/2 signaling promotes nuclear PKA activity. A-C) Nuclear ERK1/2 (A), nuclear PKA (B) and cytosolic PKA (C) activation in striatal neurons pretreated with vehicle or SCH772984 (10 nM) and treated with forskolin, phorbol 12-myristate 13-acetate (PMA), or forskolin and PMA combined. Experiments consisted of 6 (EKAR-NLS), 6 (AKAR-NLS) and 5 (AKAR-NES) biological replicates containing 16,467, 12,265 and 2,220 cells respectively. For all experiments except AKAR-NES, only medium-round nuclei were included in the analysis.

Molecular Pharmacology Fast Forward. Published on September 9, 2021 as DOI: 10.1124/molpharm.121.000290
This article has not been copyedited and formatted. The final version may differ from this version.

References

Bao, X. R., I. D. C. Fraser, E. A. Wall, S. R. Quake, and M. I. Simon (2010) Variability in G-protein-coupled signaling studied with microfluidic devices, *Biophysical Journal*, 99: 2414-22.

Bertran-Gonzalez, J., C. Bosch, M. Maroteaux, M. Matamales, D. Hervé, E. Valjent, and J.-A. Girault (2008) Opposing patterns of signaling activation in dopamine D1 and D2 receptor-expressing striatal neurons in response to cocaine and haloperidol, *J Neurosci*, 28: 5671-85.

Brami-Cherrier, K., E. Valjent, D. Hervé, J. Darragh, J. C. Corvol, C. Pages, S. J. Arthur, J. A. Girault, and J. Caboche (2005) Parsing molecular and behavioral effects of cocaine in mitogen- and stress-activated protein kinase-1-deficient mice, *J Neurosci*, 25: 11444-54.

Brewer, G. J., and J. R. Torricelli (2007) Isolation and culture of adult neurons and neurospheres, *Nature Protocols*, 2: 1490-98.

Cadwell, C. R., A. Palasantza, X. Jiang, P. Berens, Q. Deng, M. Yilmaz, J. Reimer, S. Shen, M. Bethge, K. F. Tolias, R. Sandberg, and A. S. Tolias (2016) Electrophysiological, transcriptomic and morphologic profiling of single neurons using Patch-seq, *Nature Biotechnology*, 34: 199-203.

Castagna, M., Y. Takai, K. Kaibuchi, K. Sano, U. Kikkawa, and Y. Nishizuka (1982) Direct activation of calcium-activated, phospholipid-dependent protein kinase by tumor-promoting phorbol esters, *J Biol Chem*, 257: 7847-51.

Castro, L. R., M. Brito, E. Guiot, M. Polito, C. W. Korn, D. Herve, J. A. Girault, D. Paupardin-Tritsch, and P. Vincent (2013) Striatal neurones have a specific ability to respond to phasic dopamine release, *J Physiol*, 591: 3197-214.

Chavez-Abiega, S., M. L. B. Grönloh, T. W. J. Gadella, F. J. Bruggeman, and J. Goedhart (2021) Heterogeneity and dynamics of ERK and Akt activation by G protein-coupled receptors depend on the activated heterotrimeric G proteins, *bioRxiv*: 2021.07.27.453948.

Chen, Y., A. J. Granger, T. Tran, J. L. Saulnier, A. Kirkwood, and B. L. Sabatini (2017) Endogenous Gαq-Coupled Neuromodulator Receptors Activate Protein Kinase A, *Neuron*, 96: 1070-83.e5.

Darmopil, S., A. B. Martín, I. R. De Diego, S. Ares, and R. Moratalla (2009) Genetic inactivation of dopamine D1 but not D2 receptors inhibits L-DOPA-induced dyskinesia and histone activation, *Biol Psychiatry*, 66: 603-13.

Fasano, S., A. D'Antoni, P. C. Orban, E. Valjent, E. Putignano, H. Vara, T. Pizzorusso, M. Giustetto, B. Yoon, P. Soloway, R. Maldonado, J. Caboche, and R. Brambilla (2009) Ras-guanine nucleotide-releasing factor 1 (Ras-GRF1) controls activation of extracellular signal-regulated kinase (ERK) signaling in the striatum and long-term behavioral responses to cocaine, *Biol Psychiatry*, 66: 758-68.

Flores-Hernández, J., C. Cepeda, E. Hernández-Echeagaray, C. R. Calvert, E. S. Jokel, A. A. Fienberg, P. Greengard, and M. S. Levine (2002) Dopamine Enhancement of NMDA Currents in Dissociated Medium-Sized Striatal Neurons: Role of D1 Receptors and DARPP-32, *Journal of Neurophysiology*, 88: 3010-20.

Fuzik, J., A. Zeisel, Z. Máté, D. Calvigioni, Y. Yanagawa, G. Szabó, S. Linnarsson, and T. Harkany (2016) Integration of electrophysiological recordings with single-cell RNA-seq data identifies neuronal subtypes, *Nature Biotechnology*, 34: 175-83.

Gerfen, C. R., T. M. Engber, L. C. Mahan, Z. Susel, T. N. Chase, F. J. Monsma, and D. R. Sibley (1990) D1 and D2 dopamine receptor-regulated gene expression of striatonigral and striatopallidal neurons, *Science*, 250: 1429.

Gerfen, C. R., S. Miyachi, R. Paletzki, and P. Brown (2002) D1 dopamine receptor supersensitivity in the dopamine-depleted striatum results from a switch in the regulation of ERK1/2/MAP kinase, *J Neurosci*, 22: 5042-54.

Gokce, O., Geoffrey M. Stanley, B. Treutlein, Norma F. Neff, J. G. Camp, Robert C. Malenka, Patrick E. Rothwell, Marc V. Fuccillo, Thomas C. Südhof, and Stephen R. Quake (2016) Cellular Taxonomy of the Mouse Striatum as Revealed by Single-Cell RNA-Seq, *Cell Reports*, 16: 1126-37.

Handly, L. N., J. Yao, and R. Wollman (2016) Signal Transduction at the Single-Cell Level: Approaches to Study the Dynamic Nature of Signaling Networks, *Journal of Molecular Biology*, 428: 3669-82.

Harootunian, A. T., S. R. Adams, W. Wen, J. L. Meinkoth, S. S. Taylor, and R. Y. Tsien (1993) Movement of the free catalytic subunit of cAMP-dependent protein kinase into and out of the nucleus can be explained by diffusion, *Mol Biol Cell*, 4: 993-1002.

Hoare, S. R. J., P. H. Tewson, A. M. Quinn, T. E. Hughes, and L. J. Bridge (2020) Analyzing kinetic signaling data for G-protein-coupled receptors, *Scientific Reports*, 10: 12263.

Ilouz, R., V. Lev-Ram, E. A. Bushong, T. L. Stiles, D. Friedmann-Morvinski, C. Douglas, J. L. Goldberg, M. H. Ellisman, and S. S. Taylor (2017) Isoform-specific subcellular localization and function of protein kinase A identified by mosaic imaging of mouse brain, *eLife*, 6: e17681.

Ivkovic, S., and M. E. Ehrlich (1999) Expression of the Striatal DARPP-32/ARPP-21 Phenotype in GABAergic Neurons Requires Neurotrophins In Vivo and In Vitro, *J Neurosci*, 19: 5409.

Jones-Tabah, J., H. Mohammad, S. Hadj-Youssef, L. E. H. Kim, R. D. Martin, F. Benaliouad, J. C. Tanny, P. B. S. Clarke, and T. E. Hébert (2020) Dopamine D1 receptor signalling in dyskinetic Parkinsonian rats revealed by fiber photometry using FRET-based biosensors, *Scientific Reports*, 10: 14426.

Komatsu, N., K. Aoki, M. Yamada, H. Yukinaga, Y. Fujita, Y. Kamioka, and M. Matsuda (2011) Development of an optimized backbone of FRET biosensors for kinases and GTPases, *Mol Biol Cell*, 22: 4647-56.

Mao, L., Q. Tang, S. Samdani, Z. Liu, and J. Q. Wang (2004) Regulation of MAPK/ERK phosphorylation via ionotropic glutamate receptors in cultured rat striatal neurons, *European Journal of Neuroscience*, 19: 1207-16.

Mariani, L. L., S. Longueville, J. A. Girault, D. Hervé, and N. Gervasi (2019) Differential enhancement of ERK, PKA and Ca(2+) signaling in direct and indirect striatal neurons of Parkinsonian mice, *Neurobiol Dis*, 130: 104506.

Märtin, A., D. Calvigioni, O. Tzortzi, J. Fuzik, E. Wärnberg, and K. Meletis (2019) A Spatiomolecular Map of the Striatum, *Cell Reports*, 29: 4320-33.e5.

Matamales, M., J. Bertran-Gonzalez, L. Salomon, B. Degos, J.-M. Deniau, E. Valjent, D. Hervé, and J.-A. Girault (2009) Striatal Medium-Sized Spiny Neurons: Identification by Nuclear

Staining and Study of Neuronal Subpopulations in BAC Transgenic Mice, *PLOS ONE*, 4: e4770.

Miyawaki, A. (2011) Development of probes for cellular functions using fluorescent proteins and fluorescence resonance energy transfer, *Annu Rev Biochem*, 80: 357-73.

Montero, P., and J. A. Vilar (2014) TSclust: An R Package for Time Series Clustering, *Journal of Statistical Software; Vol 1, Issue 1 (2015)*.

Muntean, B. S., S. Zucca, C. M. MacMullen, M. T. Dao, C. Johnston, H. Iwamoto, R. D. Blakely, R. L. Davis, and K. A. Martemyanov (2018) Interrogating the Spatiotemporal Landscape of Neuromodulatory GPCR Signaling by Real-Time Imaging of cAMP in Intact Neurons and Circuits, *Cell Reports*, 22: 255-68.

Pascoli, V., A. Besnard, D. Herve, C. Pages, N. Heck, J. A. Girault, J. Caboche, and P. Vanhoutte (2011) Cyclic adenosine monophosphate-independent tyrosine phosphorylation of NR2B mediates cocaine-induced extracellular signal-regulated kinase activation, *Biol Psychiatry*, 69: 218-27.

Paul, S., G. L. Snyder, H. Yokakura, M. R. Picciotto, A. C. Nairn, and P. J. Lombroso (2000) The Dopamine/D1 Receptor Mediates the Phosphorylation and Inactivation of the Protein Tyrosine Phosphatase STEP via a PKA-Dependent Pathway, *J Neurosci*, 20: 5630.

Pavón, N., A. B. Martín, A. Mendialdua, and R. Moratalla (2006) ERK phosphorylation and FosB expression are associated with L-DOPA-induced dyskinesia in hemiparkinsonian mice, *Biol Psychiatry*, 59: 64-74.

Santini, E., C. Alcacer, S. Cacciatore, M. Heiman, D. Hervé, P. Greengard, J. A. Girault, E. Valjent, and G. Fisone (2009) L-DOPA activates ERK signaling and phosphorylates histone H3 in the striatonigral medium spiny neurons of hemiparkinsonian mice, *J Neurochem*, 108: 621-33.

Saunders, A., E. Z. Macosko, A. Wysoker, M. Goldman, F. M. Krienen, H. de Rivera, E. Bien, M. Baum, L. Bortolin, S. Wang, A. Goeva, J. Nemesh, N. Kamitaki, S. Brumbaugh, D. Kulp, and S. A. McCarroll (2018) Molecular Diversity and Specializations among the Cells of the Adult Mouse Brain, *Cell*, 174: 1015-30.e16.

Savell, K. E., J. J. Tuscher, M. E. Zipperly, C. G. Duke, R. A. Phillips, A. J. Bauman, S. Thukral, F. A. Sultan, N. A. Goska, L. Ianov, and J. J. Day (2020) A dopamine-induced gene expression signature regulates neuronal function and cocaine response, *Science Advances*, 6: eaba4221.

Saxena, M., S. Williams, K. Tasken, and T. Mustelin (1999) Crosstalk between cAMP-dependent kinase and MAP kinase through a protein tyrosine phosphatase, *Nature Cell Biology*, 1: 305-11.

Schambra, U. B., G. E. Duncan, G. R. Breese, M. G. Fornaretto, M. G. Caron, and R. T. Fremeau (1994) Ontogeny of D1a and D2 dopamine receptor subtypes in rat brain using in situ hybridization and receptor binding, *Neuroscience*, 62: 65-85.

Singh, D. K., C.-J. Ku, C. Wichaidit, R. J. Steininger Iii, L. F. Wu, and S. J. Altschuler (2010) Patterns of basal signaling heterogeneity can distinguish cellular populations with different drug sensitivities, *Molecular Systems Biology*, 6: 369.

Sohn, J., M. Takahashi, S. Okamoto, Y. Ishida, T. Furuta, and H. Hioki (2017) A Single Vector Platform for High-Level Gene Transduction of Central Neurons: Adeno-Associated Virus Vector Equipped with the Tet-Off System, *PLOS ONE*, 12: e0169611.

Stanley, G., O. Gokce, R. C. Malenka, T. C. Südhof, and S. R. Quake (2020) Continuous and Discrete Neuron Types of the Adult Murine Striatum, *Neuron*, 105: 688-99.e8.

Thibault, D., F. Loustalot, G. M. Fortin, M.-J. Bourque, and L.-É. Trudeau (2013) Evaluation of D1 and D2 Dopamine Receptor Segregation in the Developing Striatum Using BAC Transgenic Mice, *PLOS ONE*, 8: e67219.

Tsou, P., B. Zheng, C.-H. Hsu, Atsuo T. Sasaki, and Lewis C. Cantley (2011) A Fluorescent Reporter of AMPK Activity and Cellular Energy Stress, *Cell Metabolism*, 13: 476-86.

Valjent, E., V. Pascoli, P. Svenningsson, S. Paul, H. Enslen, J.-C. Corvol, A. Stipanovich, J. Caboche, P. J. Lombroso, A. C. Nairn, P. Greengard, D. Hervé, and J.-A. Girault (2005) Regulation of a protein phosphatase cascade allows convergent dopamine and glutamate signals to activate ERK in the striatum, *Proc Natl Acad Sci U S A*, 102: 491.

Westin, J. E., L. Vercammen, E. M. Strome, C. Konradi, and M. A. Cenci (2007) Spatiotemporal pattern of striatal ERK1/2 phosphorylation in a rat model of L-DOPA-induced dyskinesia and the role of dopamine D1 receptors, *Biol Psychiatry*, 62: 800-10.

Yao, J., A. Pilko, and R. Wollman (2016) Distinct cellular states determine calcium signaling response, *Molecular Systems Biology*, 12: 894.

Yapo, C., A. G. Nair, L. Clement, L. R. Castro, J. Hellgren Kotaleski, and P. Vincent (2017) Detection of phasic dopamine by D1 and D2 striatal medium spiny neurons, *J Physiol*, 595: 7451-75.

Yapo, C., A. G. Nair, J. Hellgren Kotaleski, P. Vincent, and L. R. V. Castro (2018) Switch-like PKA responses in the nucleus of striatal neurons, *Journal of Cell Science*, 131: jcs216556.

Molecular Pharmacology Fast Forward. Published on September 9, 2021 as DOI: 10.1124/molpharm.121.000290
This article has not been copyedited and formatted. The final version may differ from this version.

Figure 1

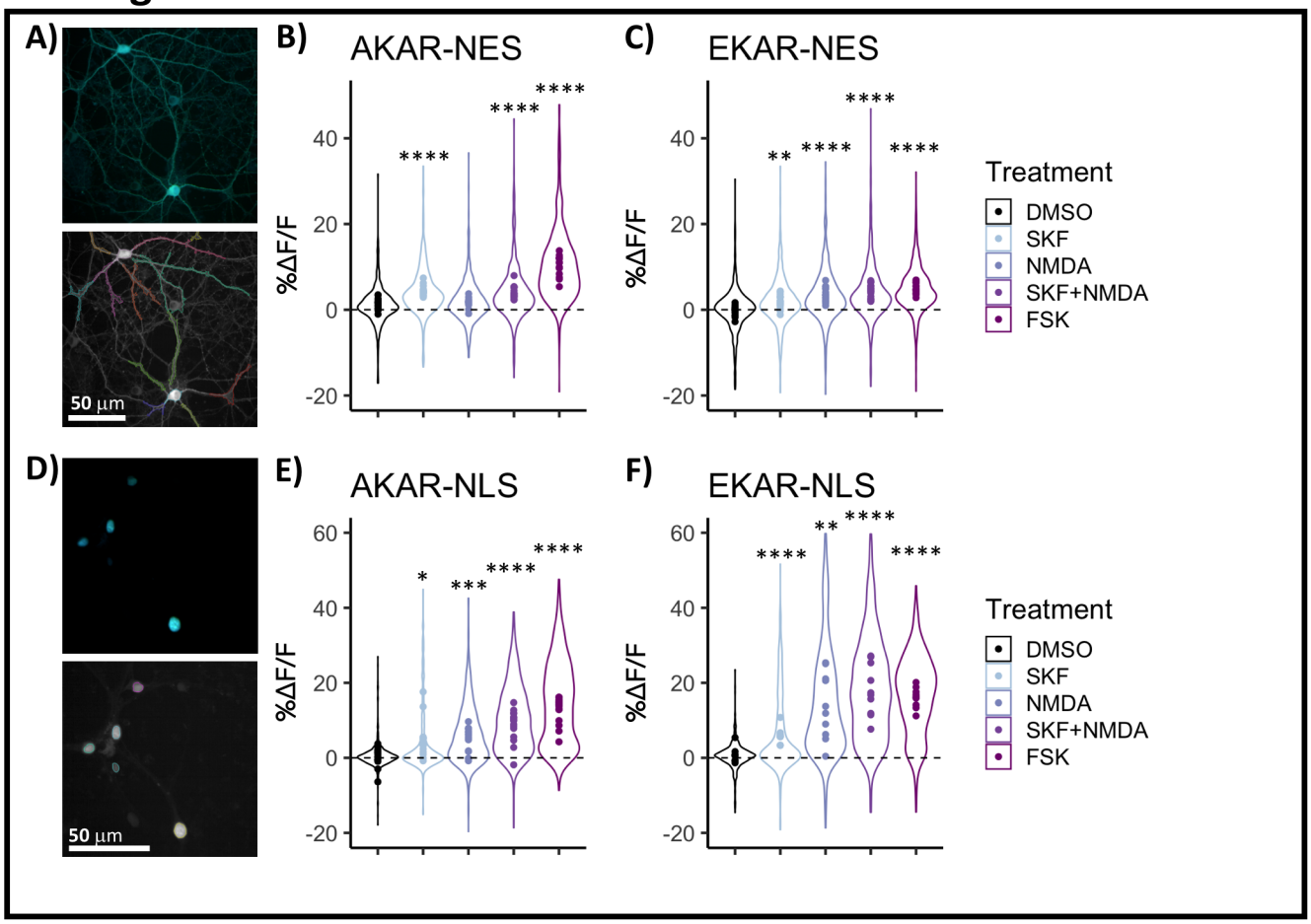

Molecular Pharmacology Fast Forward. Published on September 9, 2021 as DOI: 10.1124/molpharm.121.000290
This article has not been copyedited and formatted. The final version may differ from this version.

Figure 2

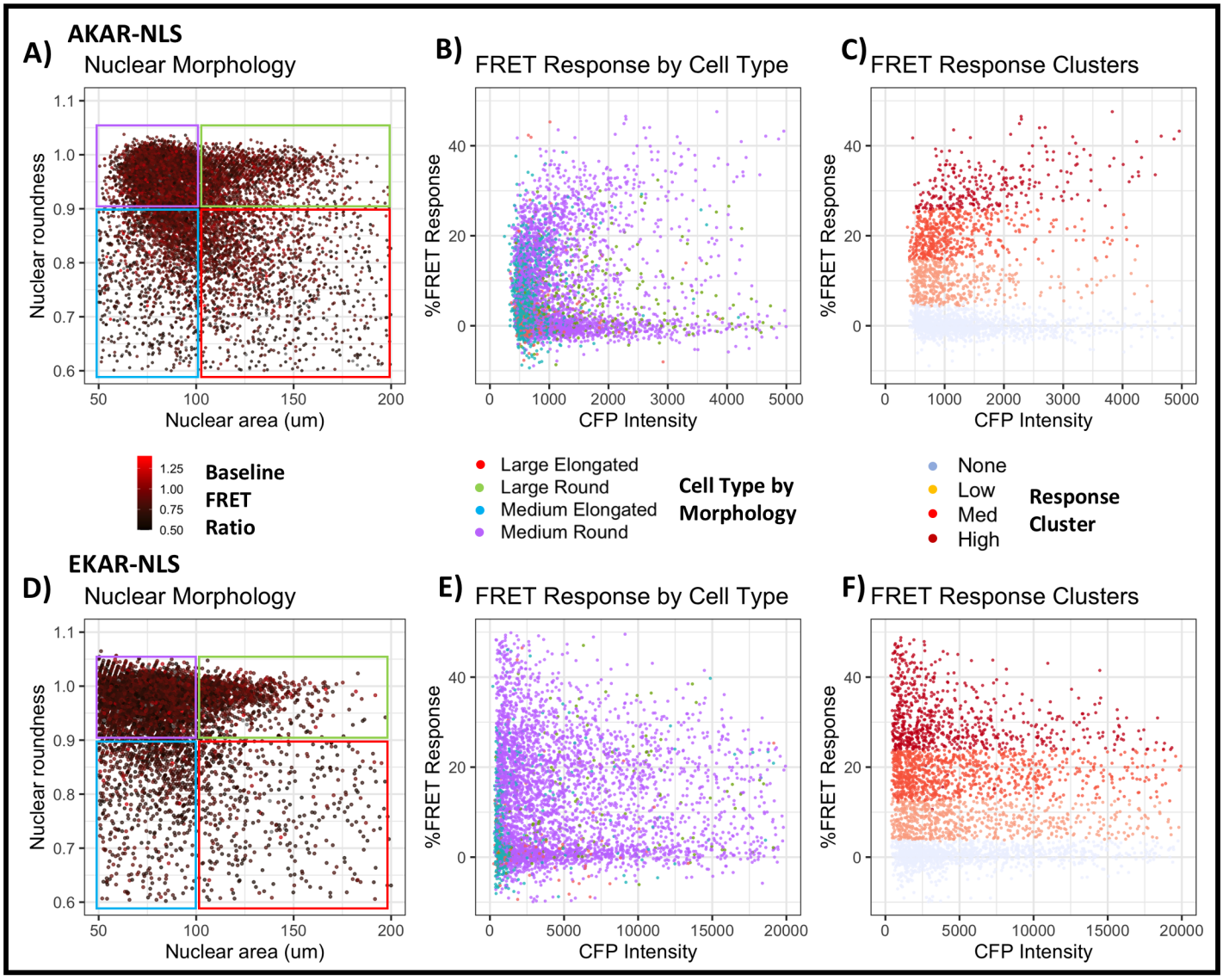

Molecular Pharmacology Fast Forward. Published on September 9, 2021 as DOI: 10.1124/molpharm.121.000290
This article has not been copyedited and formatted. The final version may differ from this version.

Figure 3

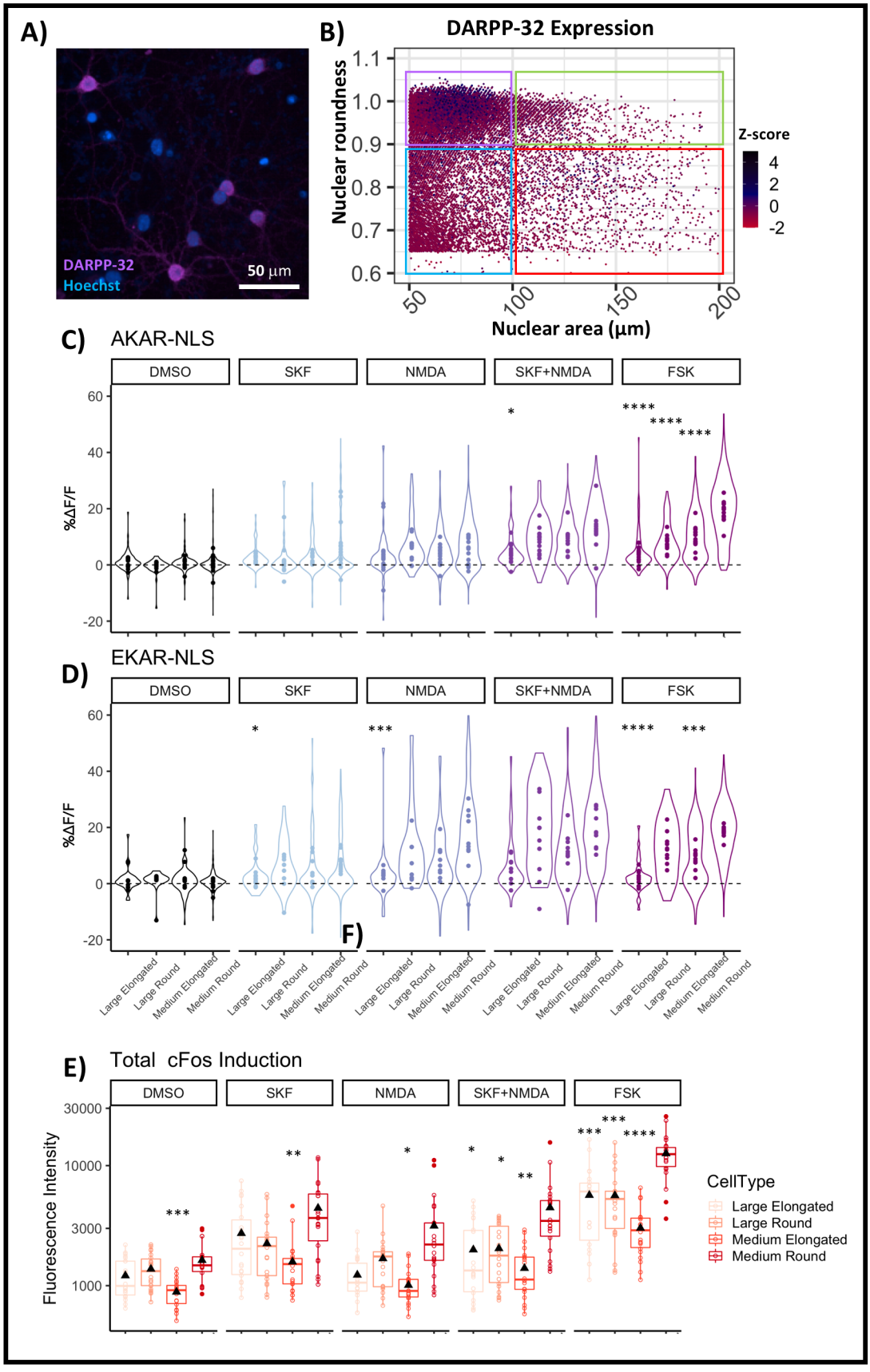

Molecular Pharmacology Fast Forward. Published on September 9, 2021 as DOI: 10.1124/molpharm.121.000290
This article has not been copyedited and formatted. The final version may differ from this version.

Figure 4

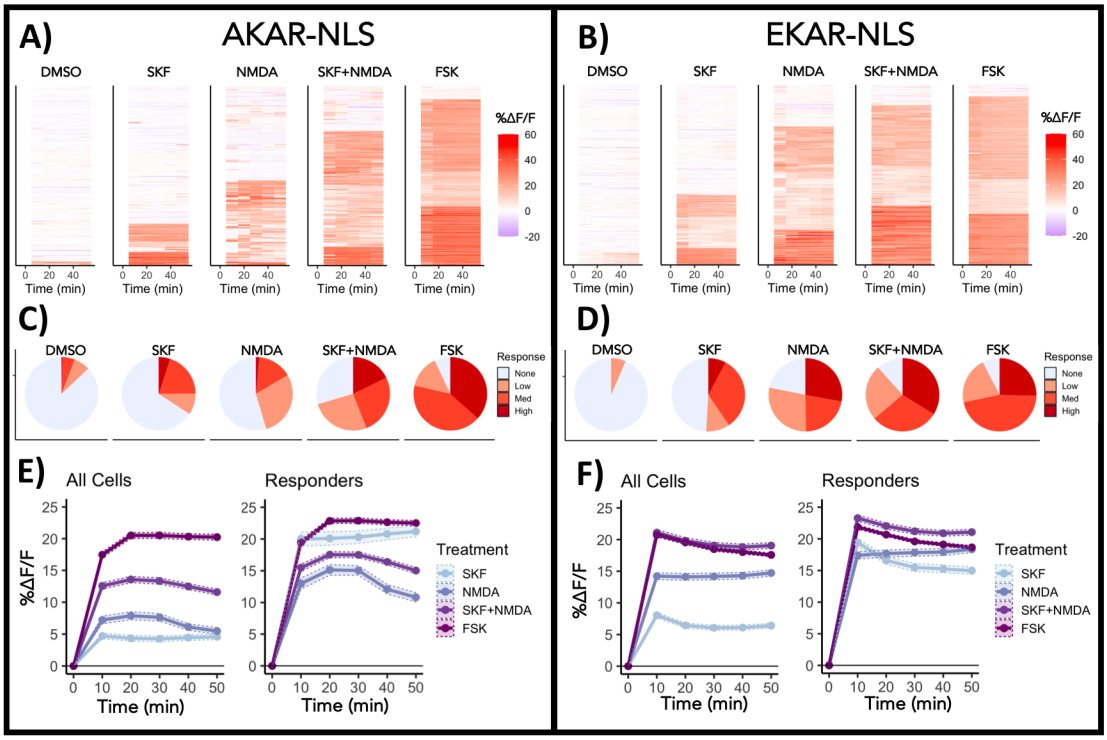

Molecular Pharmacology Fast Forward. Published on September 9, 2021 as DOI: 10.1124/molpharm.121.000290
This article has not been copyedited and formatted. The final version may differ from this version.

Figure 5

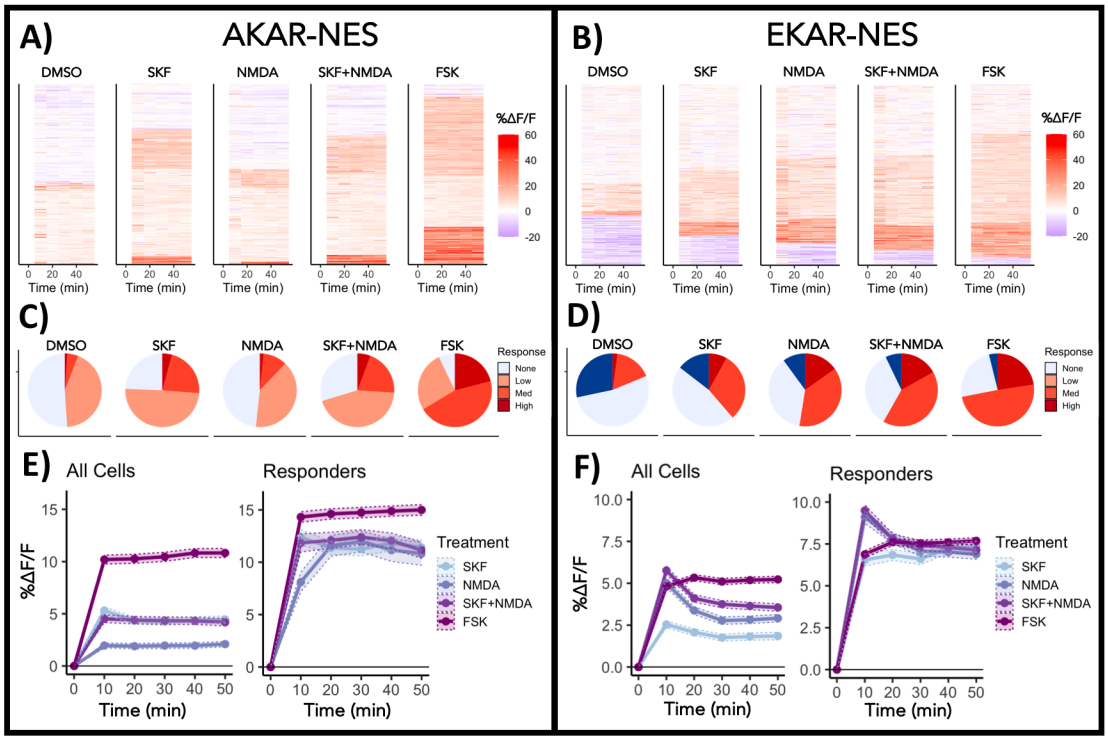

Molecular Pharmacology Fast Forward. Published on September 9, 2021 as DOI: 10.1124/molpharm.121.000290
This article has not been copyedited and formatted. The final version may differ from this version.

Figure 6

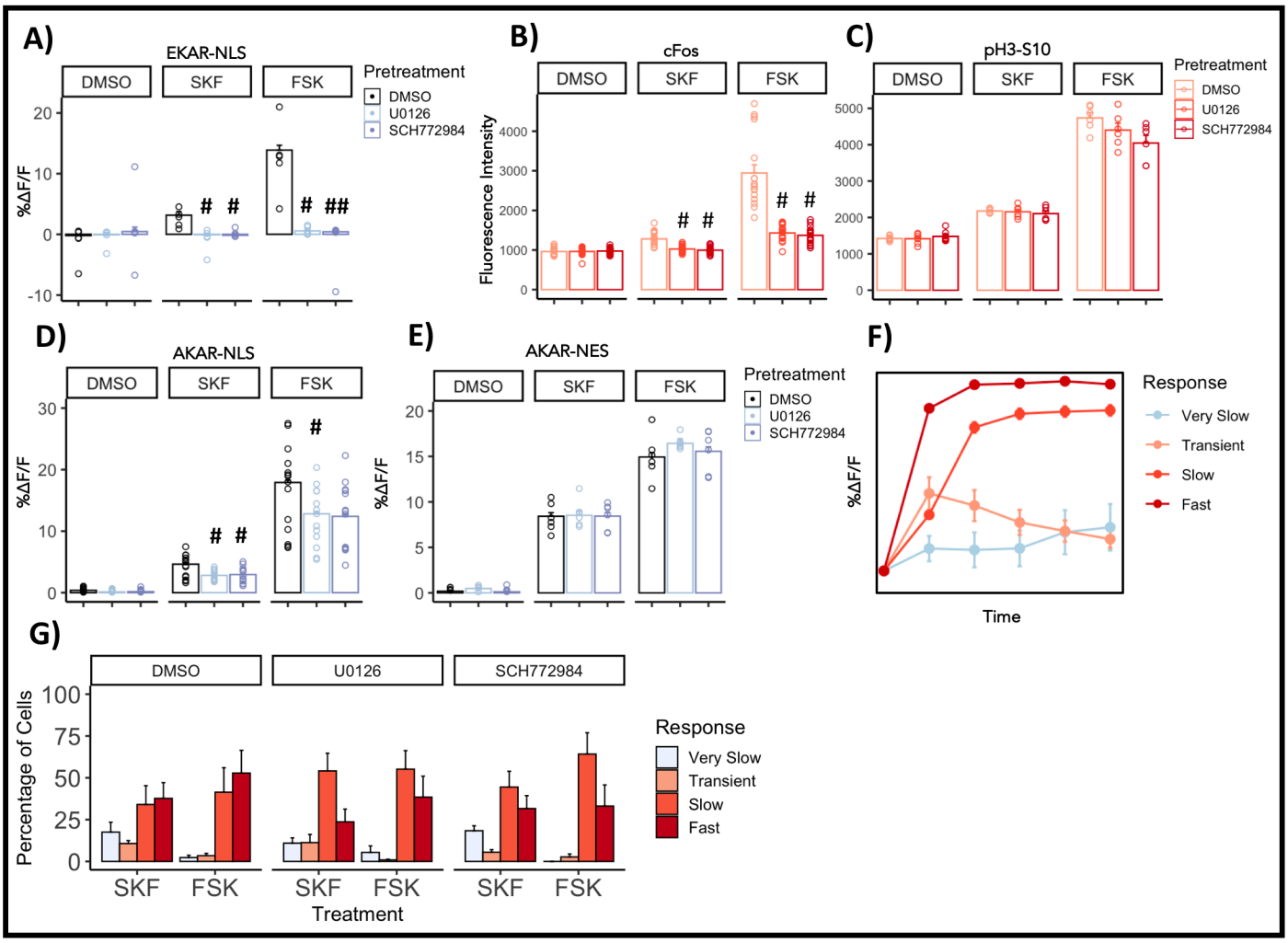

Molecular Pharmacology Fast Forward. Published on September 9, 2021 as DOI: 10.1124/molpharm.121.000290
This article has not been copyedited and formatted. The final version may differ from this version.

Figure 7

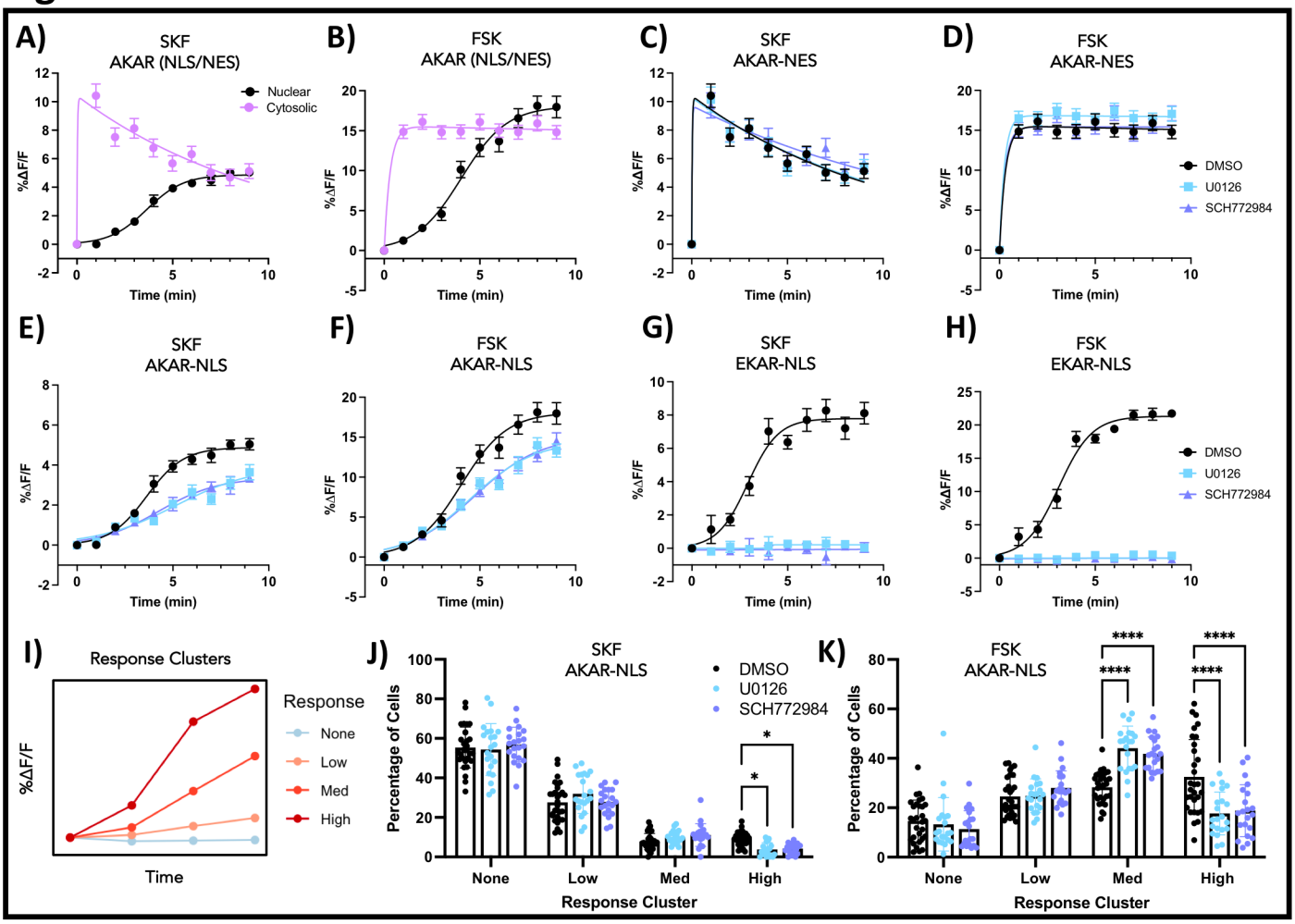

Molecular Pharmacology Fast Forward. Published on September 9, 2021 as DOI: 10.1124/molpharm.121.000290
This article has not been copyedited and formatted. The final version may differ from this version.

Figure 8

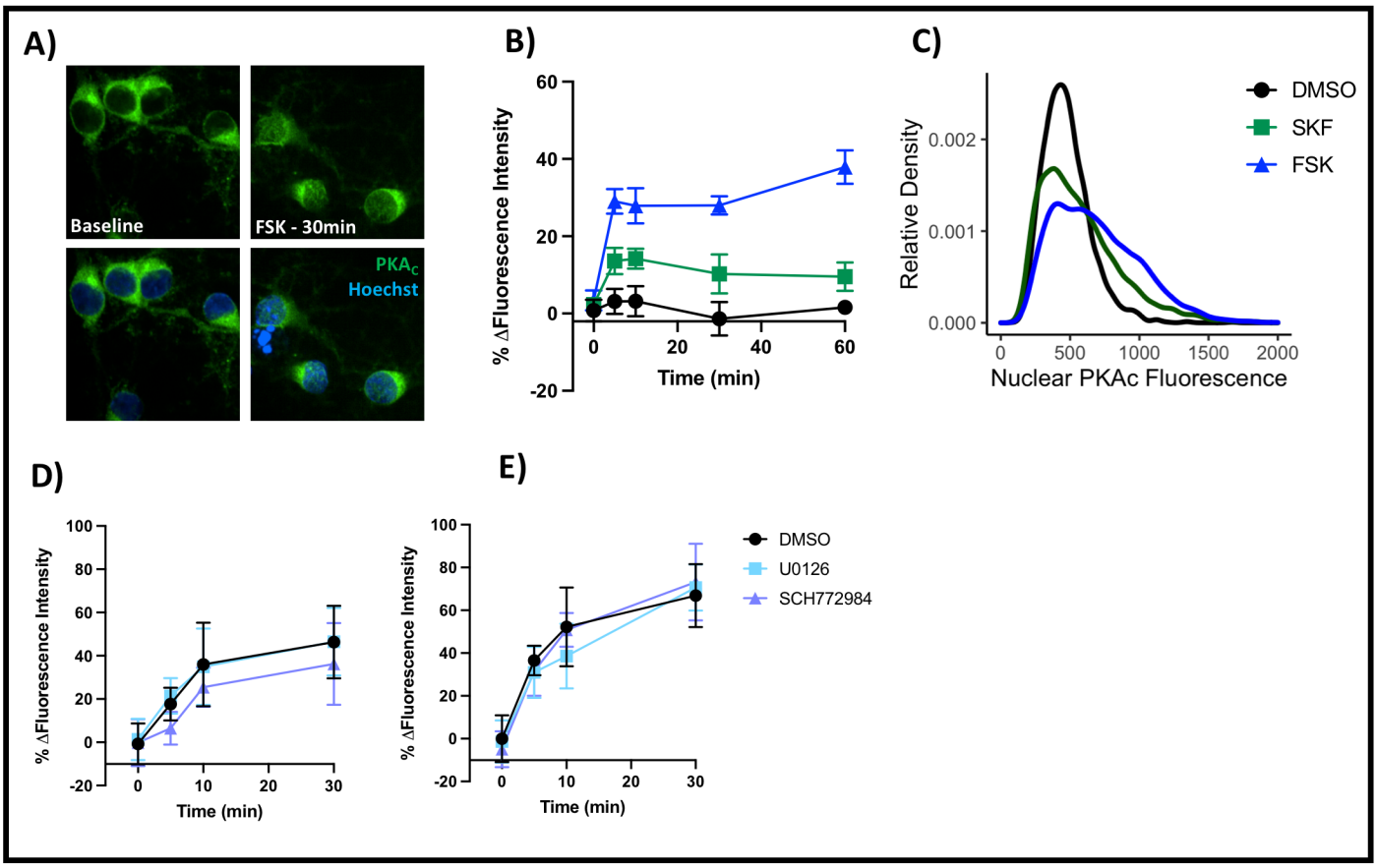

Molecular Pharmacology Fast Forward. Published on September 9, 2021 as DOI: 10.1124/molpharm.121.000290
This article has not been copyedited and formatted. The final version may differ from this version.

Figure 9

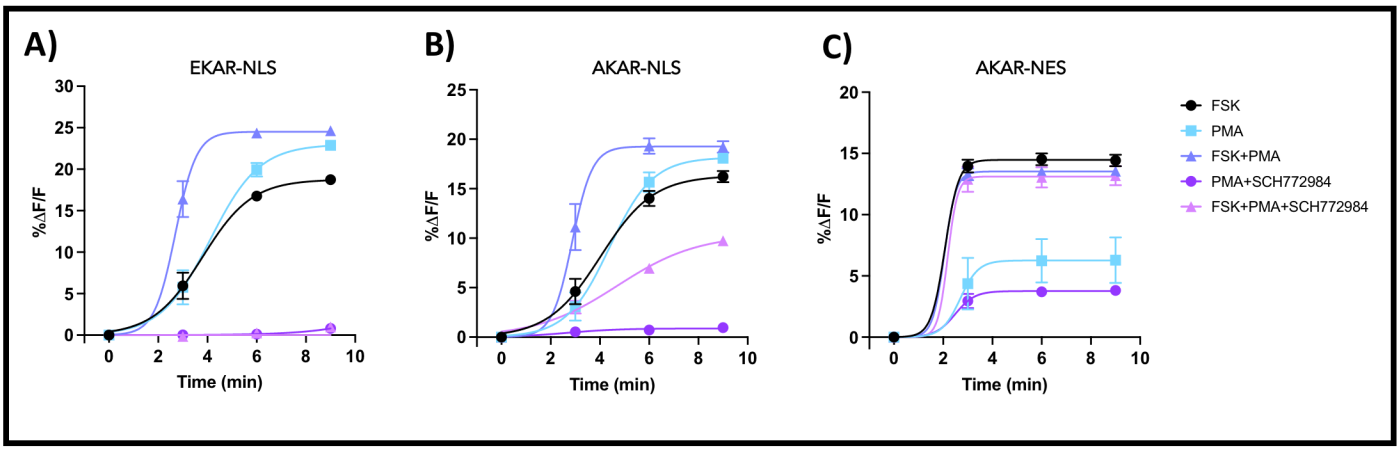

Single-cell analysis of population-wide nuclear and cytosolic drug responses using high-content FRET imaging: measuring protein kinase activation in cultured striatal neurons

Jace Jones-Tabah[1], Ryan D. Martin[1], Jason C. Tanny[1], Paul B.S. Clarke[1]* and Terence E. Hébert[1]*

[1]Department of Pharmacology and Therapeutics, McGill University, Montréal, Québec, H3G 1Y6, Canada

Supplemental Figures

Supplemental Figure 1: Expression of D1R in striatal neurons with medium round nuclei. A) Representative image of striatal neurons isolated from Drd1-Cre transgenic rats transduced with AAV expressing a Cre-dependent mCherry (AAV-DIO-mCherry). B) Nuclear morphology of Drd1-positive neurons (red dots) overlaid on the roundness *vs.* area coordinate map generated from cells immunostained for DARPP-32 shown in **Figure 3B**.

Supplemental Figure 2: Response clustering. Mean ± SEM FRET response profiles for response clusters generated in **Figure 4** and **Figure 5**. Note that most SEM bars are masked by the symbols showing the mean values.

Supplemental Figure 3: Single-cell analysis of cFos and pH3-S10 expression. A) Frequency histogram showing relative proportion of cells with the indicated levels of cFos fluorescent signal (arbitrary units), 3 hours after the indicated treatment/pretreatments. B) Percentage of cells falling into each response cluster (mean of biological replicates) for the indicated treatment/pretreatment combinations. C) Relative proportion of cells with the indicated levels of pH3-S10 fluorescent signal (arbitrary units), 60 min after the indicated treatment/pretreatments. D) Percentage of cells falling into each response cluster (mean of biological replicates) for the indicated treatment/pretreatment combinations.

Supplemental Figure 4: Single-cell analysis of nuclear PKA activation in the presence of MEK and ERK1/2 inhibitors. A-C) Single-cell FRET responses for AKAR-NLS expressing striatal neurons pretreated with vehicle, U0126 (1 μM), or SCH772984 (10 nM) and treated with SKF 81297 or forskolin.

Supplemental Figure 5: Single-cell analysis of PKA_C nuclear translocation. A) Percentage of cells falling into each response cluster (mean of biological replicates) for the indicated treatment/pretreatment combinations. B) Frequency histogram showing relative proportion of cells with the indicated levels of PKA_C fluorescent signal (arbitrary units) in the nucleus (defined by Hoechst stain), 30 min after the indicated treatment/pretreatments.

Supplemental Figure 6: Single cell analysis of PKA and ERK1/2 activation by forskolin and PMA. A-C) Percentage of cells falling into each response cluster (mean of biological replicates) for the indicated treatment/pretreatment combinations.

Supplemental Figure 1

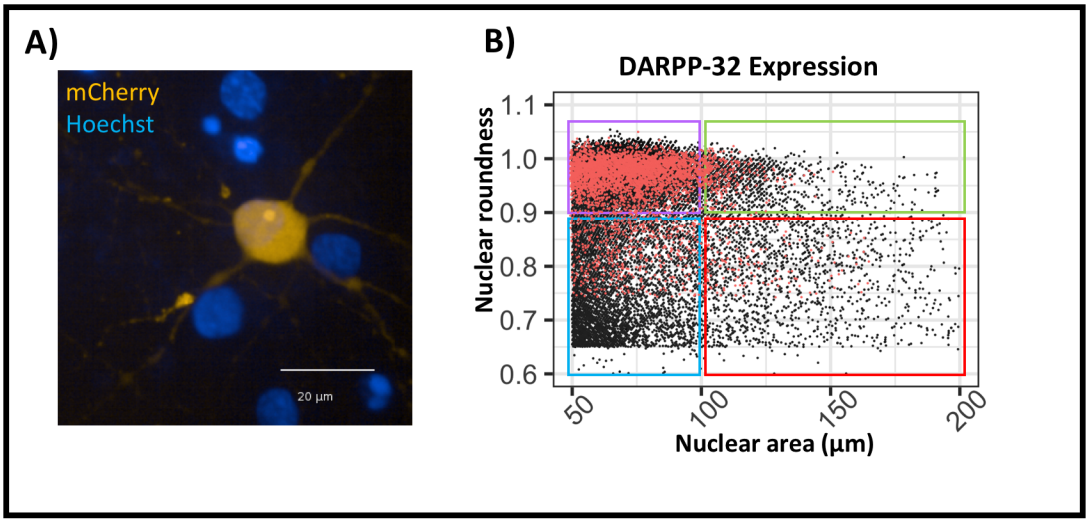

Supplemental Figure 2

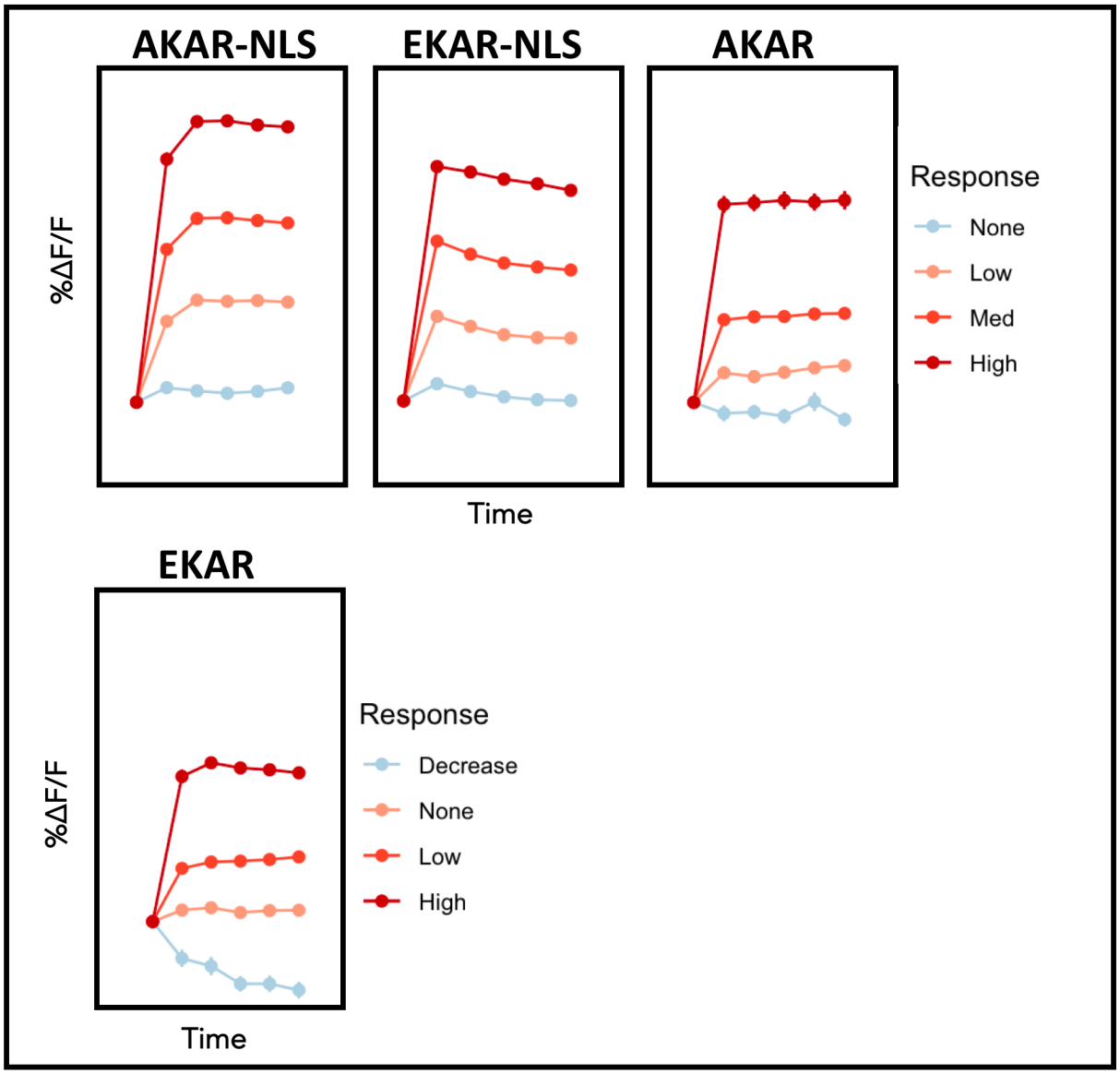

Supplementary Figure 3

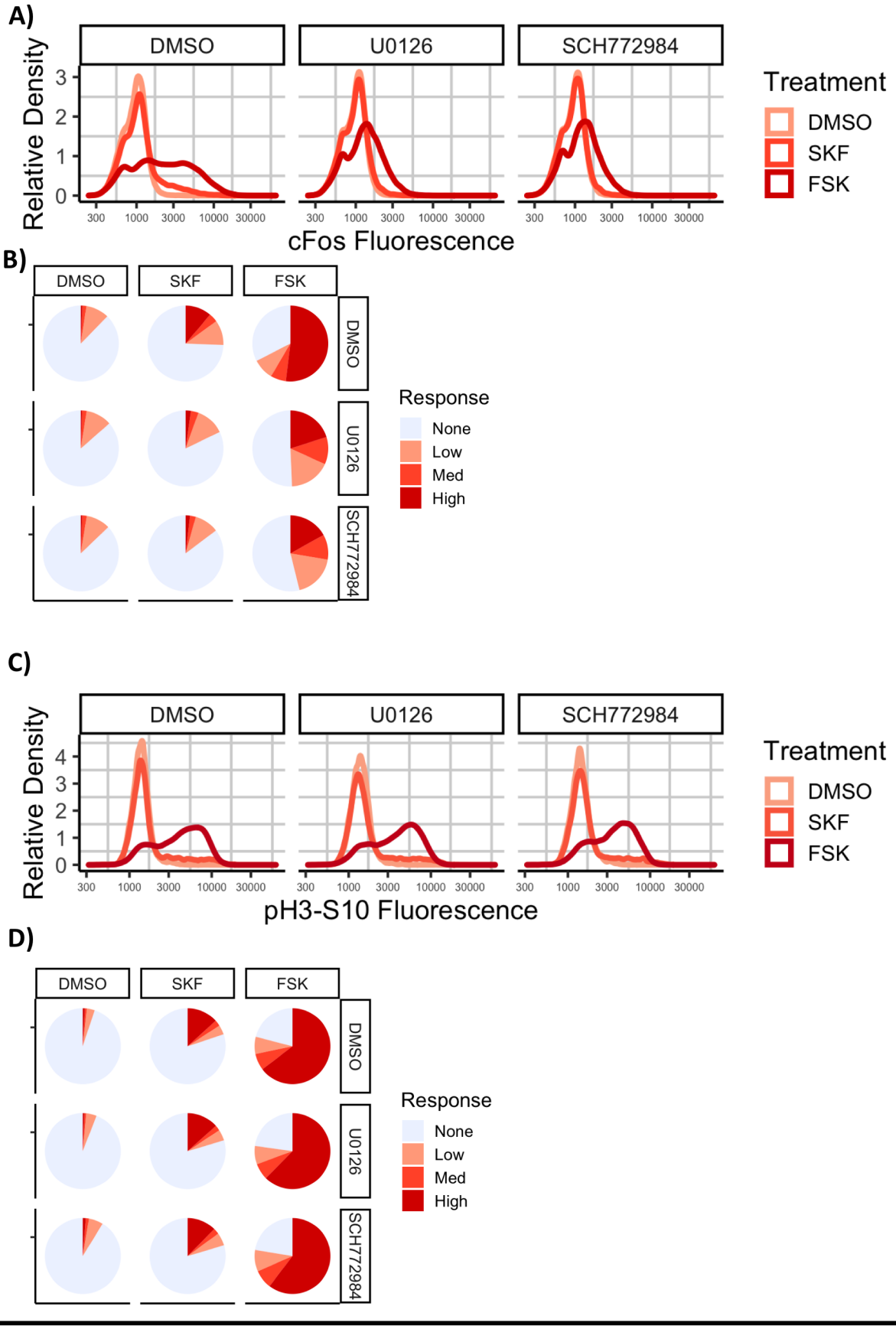

Supplemental Figure 4

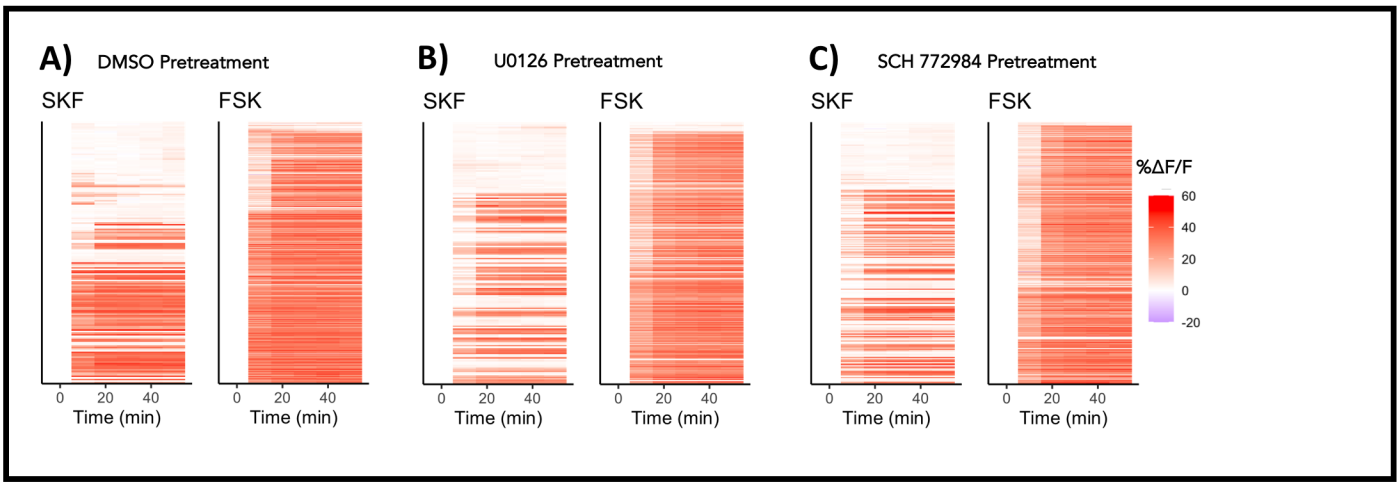

Supplemental Figure 5

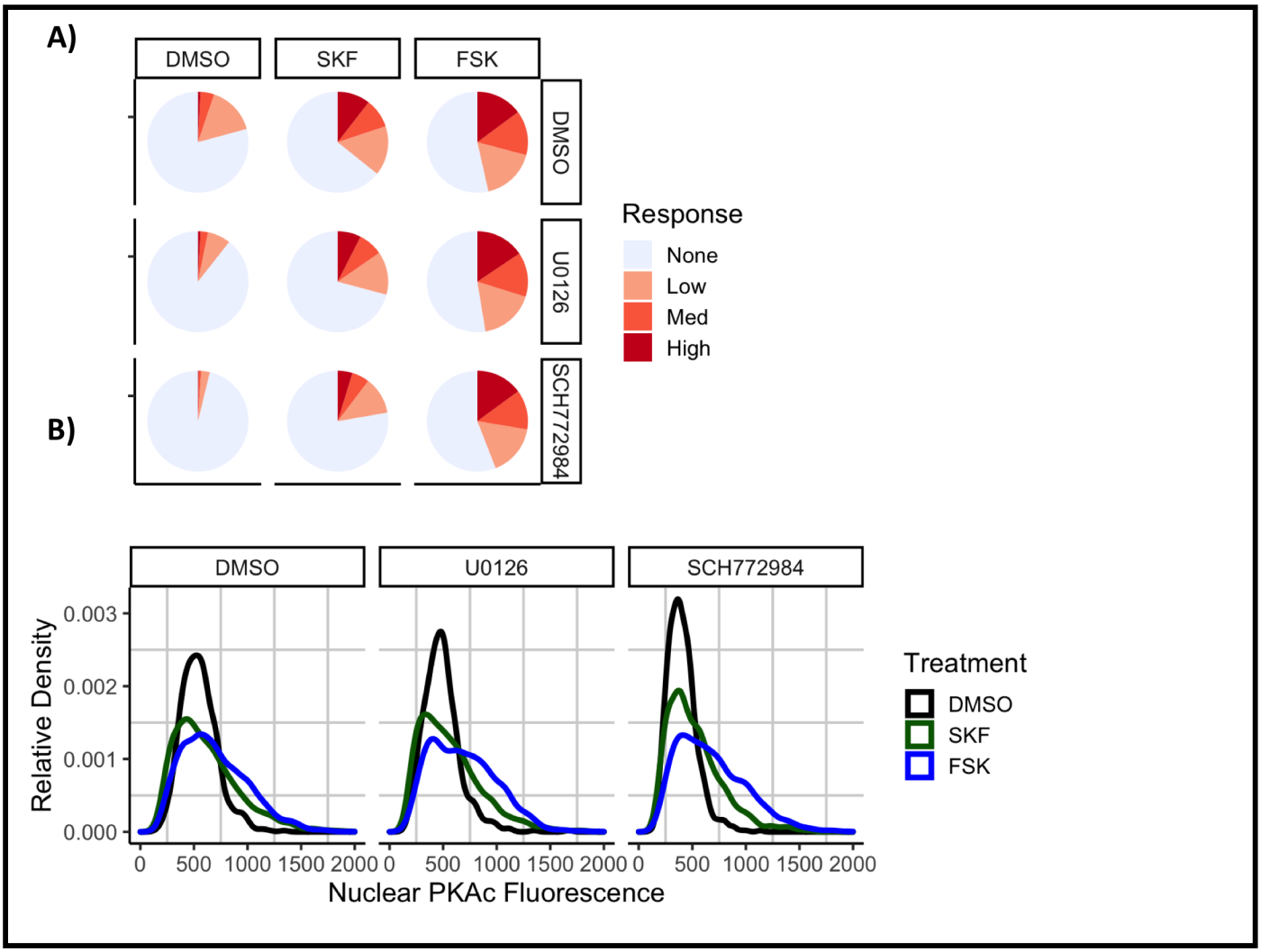

Supplemental Figure 6